Regulation of cell migration by physical stimulation and its application to tissue engineering

Min Sung Kim

Department of Medical Science

The Graduate School, Yonsei University

Regulation of cell migration by physical stimulation and its application to tissue engineering

Min Sung Kim

Department of Medical Science

The Graduate School, Yonsei University

Regulation of cell migration by physical stimulation and its application to tissue engineering

Directed by Professor Jong-Chul Park

The Doctoral Dissertation

submitted to the Department of Medical Science,

the Graduate School of Yonsei University

in partial fulfillment of the requirements for the degree of

Doctor of Philosophy of Medical Science

Min Sung Kim

December 2017

This certifies that the Doctoral Dissertation of Min Sung Kim is approved.

박 종 철

Thesis Supervisor: Jong-Chul Park

이 민 구

Thesis Committee Member#1: Min Goo Lee

박 국 인

Thesis Committee Member#2: Kook In Park

박 윤 정

Thesis Committee Member#3: Yoon-Jeong Park

황 유 식

Thesis Committee Member#4: Yu-Shik Hwang

The Graduate School

Yonsei University

December 2017

ACKNOWLEDGEMENTS

2008년 처음으로 세포제어연구실과 인연을 맺고 석사학위 과정을 시작했던 기억이 아직도 생생한데 어느덧 박사학위 졸업을 앞두게 되었다는 사실이 아직 실감이 나질 않습니다. 저 스스로 아직 부족함이 많고 배울 것이 많다고 느껴짐에도 불구하고 박사학위 졸업이 가능했던 이유는 바로 많은 분들의 도움이 있었기 때문입니다. 저 혼자만의 노력으로는 결코 이뤄낼 수 없었던 박사학위 졸업을 무사히 마칠 수 있도록 도와주신 모든 분들께 진심으로 감사의 말씀을 드립니다.

우선 존경하는 박종철 교수님께 깊은 감사를 드립니다. 항상 올바른 방향으로 저를 이끌어 주셨고 따뜻한 격려와 적절한 해결 방안을 제시해 주셨기에 제가 어려움을 극복하고 무사히 박사학위를 받을 수 있었습니다. 학술적인 면뿐만 아니라 인격적인 면에서도 많은 가르침을 받을 수 있어서 큰 기쁨이었고 영광이었습니다. 정말 감사합니다. 교수님의 가르침을 가슴 속에 새겨 넣고, 앞으로 교수님의 명성에 누를 끼치지 않도록 더욱 노력하고 성실한 자세로 모든 일에 임하는 사람이 되겠습니다.

바쁘신 와중에도 귀한 시간을 내어주신 연세대 이민구 교수님, 연세대 박국인 교수님, 서울대 박윤정 교수님, 경희대 황유식 교수님께도 깊은 감사의 말씀을 올립니다. 심사위원 교수님들의 귀중한 자문을 바탕으로 더욱 완성도 있는 학위논문을 작성할 수 있었습니다. 또한 학위과정 중 인연이 닿아 많은 깨우침을 주셨던 박봉주 교수님, 남기창 교수님, 김정구 교수님, 성학준 교수님, 김정성 교수님께도 진심으로 감사드립니다.

학위과정 중 많은 시간을 함께 보내고 실질적으로 가장 많은 도움을 주신 세포제어연구실 여러분들께 깊이 감사드립니다. 제가 말을 하도 안들어서 정말 속이 많이 썩으셨을텐데도 끝까지 저를 포기하지 않으시고 지도해주신 이미희 박사님께 진심으로 감사드립니다. 따뜻하고 세심한 배려심을 갖추신 현숙누나, 꼼꼼함과 성실함을 두루 갖춘 권병주 박사님, 멘사회원임을 실력으로 보여주는 민아, 주변에 행복한 기운을 전파하는 경미, 부족한 저를 잘 따라주었던 홍승희양, 실험실의 안방마님과 같은 착한 혜진이, 언제나 너그러운 모습으로 힘이 되어 주셨던 도현형님, 새신랑이자 예비아빠로써 정신 없으실 대형형님, 늘 친절하고 따뜻하신 태화누나, 자주 보지는 못했지만 늘 많은 도움을 준 형수진 박사님, 이 모든 분들의 도움으로 무사히 학위과정을 마칠 수 있었습니다. 정말 감사합니다.

사랑하는 저희 가족 모두에게 감사드립니다. 힘이 들 때마다 버팀목이 되어주신 부모님, 부족함이 많은 저를 늘 따뜻하게 대해주시고 용기를 북돋아 주신 장모님, 두 아이의 아버지로써 든든한 가장역할을 하고 있는 멋진 처남, 한참 어리지만 나보다 어른스러운 동생, 모두 사랑하고 고맙습니다. 마지막으로 부족한 저를 이해해주고 변함없는 사랑과 믿음으로 지지해주는 사랑하는 아내 세라, 항상 고맙고 미안하고 사랑해. 그리고 우리 이쁜 딸 효은, 태어나줘서 너무나 고맙고 사랑한다. 항상 건강하고 행복하렴. 아빠가 많이 노력할게. 정말 많이 사랑해.

모든 분들께 받은 격려와 도움을 평생 잊지 않고 항상 노력하며 앞으로 성실하게 살아가겠습니다. 정말 감사합니다.

TABLE OF CONTENTS

LIST OF FIGURES

Abstract

Regulation of cell migration by physical stimulation and its application to tissue engineering

Min Sung Kim

Department of Medical Science

The Graduate School, Yonsei University

(Directed by Professor Jong-Chul Park)

In tissue engineering, the scaffold is fabricated using bioactive factors and biomaterials to give the extracelluar matrix environment to the wounded area. In recent years there have been tremendous studies in the stem cell therapy, because it has some advantages which can restore function to damaged or diseased tissue, specifically adult stem cells, multipotent cells with the

capacity to promote angiogenesis, differentiate to produce multiple types of connective tissue.

There are some important issues when we use the scaffold and stem cells for tissue engineering and regenerative medicine. The first issue is homogeneous distribution in the scaffold and the second issue is cell homogeneity in stem cell culture. To find out about the possibility to solve these issues, the cell migration control technology using physical stimulations was dealt with in this study. The chemical stimulation could affect the cell migration too; however, it is not easy to remove the influence of the residual chemical. Therefore physical stimulations; fluid shear stress and electric current will be identified to control the cell migration for tissue engineering and cell therapy.

For fluid shear stress experiment, the parallel plate chamber system was used. The gold patterned glass system and agar-salt bridge system were used for electric current experiments. All migration data were analysed by Image J software. The fluid shear stress induced the directional migration along the fluid direction and enhanced the migration of hMSCs into the poly(lactic-co-glycolic acid) scaffold. In electrotaxis study, directional migration of nHDFs and stem cells was controlled and infiltration into scaffold

was enhanced. Also, adipose derived stem cells, human mesenchymal stem cells, tonsil mesenchymal stem cells and osteogenic differentiated cells were migrated toward anode however the migration speed of osteogenic differentiated cells were significantly decreased. In conclusion, fluid shear stress and electric current induced directional cell migration, and also enhanced cell infiltration into scaffolds. As a result, we suggest that the physical stimulation could easily control the cell migration and be applicable in tissue engineering and cell therapy.

Keywords: cell migration, 3-D scaffold, tissue engineering, stem cell, electrotaxis, fluid shear stress, cell homogeneity

Regulation of cell migration by physical stimulation and its application to tissue engineering

Min Sung Kim

Department of Medical Science

The Graduate School, Yonsei University

(Directed by Professor Jong-Chul Park)

I. Introduction

1. Tissue engineering and regenerative medicine

The current demands for transplant organs and tissues is far outpacing the supply, and all manner of projections indicate that this gap will continue to widen.[1,2] Cell transplantation has recently been proposed as an alternative treatment to whole organ

transplantation for failing or malfunctioning organs.[3-5] For the creation of an autologous implant, donor tissue is harvested and dissociated into individual cells, and the cells are attached and cultured onto a proper substrate that is ultimately implanted at the desired site of the functioning tissue. In recent years there have been tremendous studies in the stem cell therapy, because it has some advantages which can restore function to damaged or diseased tissue, avoid host rejection and reduce inflammation throughout the body without the use of immunosuppressive drugs.[6] However, it is believed that the cells cannot form new tissues by themselves. Most primary organ cells are believed to be anchorage-dependent and require specific environments that very often include the presence of a supporting material to act as a template for growth. The success of any cell transplantation therapy therefore relies on the development of suitable substrates for both in vitro and in vivo tissue culture. Currently, these substrates, mainly in the form of tissue engineering scaffolds, prove less than ideal for applications, not only because they lack mechanical strength, but they also suffer from a lack of interconnection channels.

Tissue engineering, an important emerging topic in biomedical

engineering, has shown tremendous promise in creating biological alternatives for harvested tissues, implants, and prostheses.[7] The underlying concept of tissue engineering is the belief that cells can be isolated from a patient, and its population then expanded in a cell culture and seeded onto a carrier. The resulting tissue engineering construct is then grafted back into the same patient to function as the introduced replacement tissue. In this approach, a highly porous artificial extracellular matrices,[8] or scaffold, is thought to be needed to accommodate mammalian cells and guide their growth and tissues regeneration in three dimensions.

A scaffold is one of the key components in the tissue engineering paradigm in which it can function as a template to allow new tissue growth and also provide temporary structural support while serving as a delivery vehicle for cells and/or bioactive molecules.[3,9]An ideal scaffold for tissue regeneration should possess mechanical properties similar to the tissues being replaced, good biocompatibility with surrounding tissue, large porosity and pore size for good infiltration of cells, high pore interconnectivity for tissue ingrowth, and biodegradability such that it is gradually replaced by growing tissues.[10] For a scaffold that requires minimal cellular infiltration (e.g., a vascular graft) and proliferation limited

to the surface may be acceptable or even desirable. A large number of studies have been devoted to characterize the in vitro new tissue regeneration capability of hMSCs cultured within biodegradable porous scaffolds. The results of these studies evidenced that parameters such as surface topography and chemistry as well as hMSC seeding density and three dimension (3-D) spatial distribution/organization strongly influence cell-material interaction and extracellular matrix deposition.[11-16] Nevertheless, cell cultivation in 3-D porous scaffolds is often impaired by the difficulty of achieving a homogeneous cell seeding and by the diffusion constraints within the cell-scaffold constructs.[13,16-18]The cells widely distributed on the scaffolds could give the appropriate mechanical strength and degradation rates to the scaffolds, especially hard tissue scaffold.[1,9]

There were many studies for enhancing the migration into the scaffold by modulation of scaffolds. The electrospun nanofibers have large surface area to volume ratio, which allows for the direct attachment of ECM ligands, growth factors and other biomolecules onto fiber surfaces to locally modulate cell and tissue function and to guide and enhance regeneration. Although the patterning of the nanofibers has been shown to influence the alignment of cells and

cellular processes,[19-23] the effects of patterned and bioactive nanofibers on cellular migration and dermal wound healing have not been fully elucidated, especially with regard to the infiltration of cells into 3-D scaffolds. One limitation of electrospun nanofibrous scaffolds is the relatively small pore size (in comparison to the average diameter of most cells) and the resultant difficulty for cell infiltration into the 3-D structure, which retards matrix remodeling and tissue regeneration. Recently, salt-leaching methods have been used to increase the pore size of the electrospun scaffolds,[24] but these methods still face the problems of collapse of fibrous structure after removing the salt. The porous, degradable poly(2-hydroxyethyl methacrylate) hydrogel scaffolds with well-defined architectures were designed using a unique photolithography process and optimized polymer chemistry. This technique may easily be expanded to other photopolymerizable chemistries in which the polymerization kinetics under different light intensities allow for patterning, however it was hard to make the homogeneous porous scaffold so cell distributed heterogeneously.[25] Rapid prototyping (RP) is one of the most promising techniques for designing and producing scaffolds for tissue engineering applications.[26-32] The scaffolds are usually characterized by their 100% interconnected pores, fully computer

controlled architecture and high porosities, which facilitate nutrient perfusion, essential to ensure cell viability. However, these techniques also present some drawbacks, including low resolution, which only allows fabrication of scaffolds with large pore sizes compared with the dimensions of a cell. This often leads to low cell seeding efficiencies (25–40%) and to a non-uniform distribution of cells along the scaffolds.[33]

2. Control of cell migration study in tissue engineering

Although these techniques have laid the foundation for generating porous structures for a variety of tissue engineering applications, they do not provide control over the pore structure, size or interconnectivity. To solve these problems, we suggested the cell migration control beside the modulation of scaffold itself. If the control of cell migration is possible, then we can enhance the cell infiltration into the scaffold, and induce the homogeneous distribution in scaffold.

One reason why cells migrate is in response to chemical mediators such as chemokines, a process called chemotaxis.[34] Chemotaxis could induce the directional migration of the cells; however, it is not easy to remove the influence of the first treated chemical when the second chemical is acting on the cells which are already affected by the first chemical to change the direction of the migration.[35] Chemotaxis is focused on the enhancing of cell migration rather than the control of directional migration. Previous study showed that chemotactic migration of the cells in the 3-D matrix in the presence of the chemoattractant.[36] The orientation of the cell migration was examined by the under-agarose cell migration assay as the cells were seeded between the control

collagen gel and platelet derived growth factor-bb (PDGF-bb) containing collagen gel. The migration of dental pulp cells were increased significantly by 50 ng/ml of the PDGF-bb, however the diffusion direction of PDGF-bb was difficult to control.[36] The migration of mouse bone-marrow-derived dendritic cells was induced by lymph node-derived chemokines CCL19, and the cells also migrated toward CCL19 in two-photon polymerized scaffold which has 50 μm, 75 μm of pore size. In this case, however the migration of cells which were outside of scaffold were enhanced more than that of cells inside of scaffold. As a result, chemotactic diffusion was not delivered into the scaffold homogeneously.[37] The migration of human mesenchymal stem cells in PCL scaffold were induced by the stromal cell-derived factor 1 (SDF-1) in vitro study, and cells migrated into the one half of scaffold for 30 days after subcutaneous implantation of 3-month-old male Wistar rats. However, the wound for the implantation of pump and tube system which is connected to the PCL scaffold to supply the SDF-1 to cells was bigger than the wound size of implantation of cell seeded PCL scaffold.[38] According to these results, the chemotaxis would enhancement of migration into scaffold but there were disadvantages for migration control such as the difficulty of directional diffusion, different chemokines for different cell types.

Therefore physical stimulations; fluid shear stress and electric current were identified to control the cell migration for tissue engineering and cell therapy.

Our previous about migration showed that the migration speed was different from the cell sources and the surface coated with different extracellular matrix (ECM) also affected to migration speed.[39,40] The cultured fetal fibroblasts moved faster that neonatal fibroblast on the I collagen, and in fibronectin, hyaluronic acid.[39] The migration distance of MC3T3-E1 cell on 0.01% type I collagen or 0.01% fibronectin was longer than that on 100 μm/ml laminin-coated glass. The migration speed on fibronectin-coated glass was 68 μm/h and this was the fastest. The migration speed on type I collagen-coated glass was similar with that on fibronectin-coated glass. The latter two migration speeds were faster than that on no-coated glass. The average migration speed on laminin-coated glass was 37 μm/h and not different from that of control group. As a result, the extracelluar matrix ligands such as type I collagen and fibronectin seem to play an important role in cell migration. The type I collagen or fibronectin coated scaffold is more effective for migration of osteoblast in tissue engineering process.[40]

3. Cell homogeneity evaluation

According to these studies, it could be possible to apply the migration analysis as an index of cell characteristic for evaluation of cell homogeneity in tissue engineering. In tissue engineering and regenerative medicine, the stem cells are differentiated to the target cells and in this point how many stem cells are differentiated to target cells is very important. Because there is a risk that undifferentiated cells could form a tumor when cells are implanted into the body. Human embryonic stem cells (HESCs) share cellular and molecular phenotypes with tumour cells and cancer cell lines.[41] Among these are rapid proliferation rate, lack of contact inhibition, a propensity for genomic instability as well as high activity of telomerase, high expression of oncogenes such as MYC and KLF4, and remarkable similarities in their overall gene expression patterns, microRNA (miRNA) signatures and epigenetic status. When injected into immunodeficient mice, HESCs form teratomas5. These tumours are so characteristic of HESCs that they have become the most stringent test for pluripotency in human cells. Indeed, treatment attempts with embryonic stem cells in animal models were shown to be fatal owing to the formation of teratoma-like tumours.[41] Undifferentiated mouse embryonic stem

cells (ES) cells consistently formed cardiac teratomas in nude or immunocompetent syngeneic mice. Cardiac teratomas contained no more cardiomyocytes than hind-limb teratomas, suggesting lack of guided differentiation. ES cells also formed teratomas in infarcted hearts, indicating injury-related signals did not direct cardiac differentiation. Allogeneic ES cells also caused cardiac teratomas, but these were immunologically rejected after several weeks, in association with increased inflammation and up-regulation of class I and II histocompatibility antigens.[42] To solve these problems, the homogeneity of scells needed to be identified before the application and the evaluation technique of stem cell homogeneity is strongly demanded.

References

1. Richmond VA. Scientific Registry for Organ Transplantation and the Organ Procurement and Transplant Network. Annual Report 1990;10:13-9.

2. Cohen S, Bano MC, Cima LG. Design of synthetic polymeric structures for cell transplantation and tissue engineering. Clin Mater 1993;13:3-10.

3. Langer R, Vacanti JP. Tissue engineering: the design and fabrication of living replacement devices for surgical reconstruction and transplantation. The Lancet 1999;354:s32-4.

4. Cima LG, Vacanti JP, Vacanti C. Tissue engineering by cell transplantation using degradable polymer substrates. J Biomech Eng 1991;113:143-51.

5. Cima LG, Ingber D, Vacanti JP. Hepatocyte culture on biodegradable polymeric substrates. Biotechnol Bioeng 191;38:145-52.

6. Ankrum J, Karp JM. Mesenchymal stem cell therapy: Two

steps forward, one step back. Trends Mol Med 2010;16: 203-9.

7. Mooney DJ, Mikos AG. Growing new organs. Sci Am 1999;38:14-22.

8. Peters MC, Mooney DJ. Synthetic extracellular matrices for cell transplantation. Mater Sci 1997;250:43-56.

9. Mistry AS, Mikos AG, Tissue engineering strategies for bone regeneration. Adv Biochem Eng Biotechnol 2005;94:1-22.

10. Xinfeng S, Balaji S, Quynh P, Feng L, Mikos AG. Fabrication of porous ultrashort single-walled carbon nanotube nanocomposite scaffolds for bone tissue engineering. Biomaterials 2007;28:4078-90.

11. Bruder SP, Fink DJ, Caplan AJ. Mesenchymal stem cells in bone development, bone repair and skeletal regeneration therapy. J Cell Biochem 1994;56:283-94.

12. Prockop DJ. Marrow stromal cells as stem cells for nonhematopoietic tissues. Science 1997;276:71-4.

13. Katsumi A, Orr W, Tzima E, Schwartz MA. Integrins in

mechanotransduction. J Biol Chem 2004;279:12001-4.

14. Huang H, Kamm RD, Lee RT. Cell mechanics and mechanotransduction: pathways, probes, and physiology. J Physiol Cell Physiol 2004;287:C1-11.

15. Song L, Peter B, Yingxiao W, Yingli H, Shunichi H. The role of the dynamics of focal adhesion kinase in the mechanotaxis of endothelial cells. Proc Natl Acad Sci U S A 2009;99:3546-51.

16. Tu ML, Wang HQ, Sun XD, Chen LJ, Ke ZJ. Pim-1 is upregulated by shear stress and is involved in shear stressinduced proliferation of rat mesenchymal stem cells. Life Sci 2011;88:233-8.

17. Yourek G, McCormick SM, Mao JJ, Reilly GC. Shear stress induces osteogenic differentiation of human mesenchymal stem cells. Regen Med 2010;5: 713-24.
18. Huang Y, Jia X, Bai K, Gong X, Fan Y. Effect of fluid shear stress on cardiomyogenic differentiation of rat bone marrow mesenchymal stem cells. Arch Med Res 2010;41:497-505.
19. Hashi CK, Zhu Y, Yang GY, Young WL, Hsiao BS, Wang K, et al. Antithrombogenic property of bone marrow

mesenchymal stem cells in nanofibrous vascular grafts. Proc Natl Acad Sci U S A 2007;104:11915-20.

20. Huang NF, Patel S, Thakar RG, Wu J, Hsiao BS, Chu B, et al. Myotube assembly on nanofibrous and micropatterned polymers. Nano Lett 2006;6:537-42.

21. Patel S, Kurpinski K, Quigley R, Gao H, Hsiao BS, Poo MM, et al. Bioactive nanofibers: synergistic effects of nanotopography and chemical signaling on cell guidance. Nano Lett 2007;7:2122-8.

22. Xu CY, Inai R, Kotaki M, Ramakrishna S. Aligned biodegradable nanofibrous structure: a potential scaffold for blood vessel engineering. Biomaterials 2004;25:877-86.

23. Yang F, Murugan R, Wang S, Ramakrishna S. Electrospinning of nano/micro scale poly(L-lactic acid) aligned fibers and their potential in neural tissue engineering. Biomaterials 2005;26:2603-10.

24. Nam J, Huang Y, Agarwal S, Lannutti J. Improved cellular infiltration in electrospun fiber via engineered porosity. Tissue Eng 2007;13:2249-57.

25. Bryant SJ, Cuy JL, Hauch KD, Ratnera BD. Photo-patterning of porous hydrogels for tissue engineering. Biomaterials 2007;28:2978-86.

26. Yeong WY. Rapid prototyping in tissue engineering: challenges and potential. Trends Biotechnol 2004;22:643-52.

27. Lee J. Three-dimensional cell culture matrices: state of the art. Tissue Eng Part B Rev 2008;14:61-86.

28. Hutmacher DW. Scaffold-based tissue engineering: Rationale for computer-aided design and solid free-form fabrication systems. Trends Biotechnol 2004;22:354-62.

29. Hutmacher DW, Cool S. Concepts of scaffold-based tissue engineering–the rationale to use solid free-form fabrication techniques. J Cell Mol Med 2007;11:654-69.

30. Hutmacher DW. Scaffolds in tissue engineering bone, cartilage. Biomaterials 2000;21:2529-43

31. Zein I. Fused deposition modeling of novel scaffold architectures for tissue engineering applications. Biomaterials 2002;23:1169-85.

32. Leong KF. Solid freeform fabrication of three-dimensional scaffolds for engineering replacement tissues and organs. Biomaterials 2003;24:2363-78.

33. Pfister A. Biofunctional rapid prototyping for tissue-engineering applications: 3D bioplotting versus 3D printing. J Polym Sci Part A: Polym Chem 2004;42:624-38.

34. Miyagi T, Chuang F, Lam K. Opioids suppress chemokine-mediated migration of monkey neutrophils and monocytes – an instant response. Immunopharmacology 2000;47: 53-62.

35. Robinson K, Messerli M. Left/right, up/down: the role of endogenous electrical fields as directional signals in development, repair and invasion. Bioessays 2003;25: 759-66.

36. You KE, Kim D, Kwon BJ, Vagaska B, Kang JK, Seo HJ, et al. Methods for Evaluation of the Chemotactic Migration of the Cells in 3D Biomimetic Matrix. Biomaterials Research 2012;16: 129-34.

37. Tayalia P, Mazur E, Mooney DJ. Controlled architectural and chemotactic studies of 3D cell migration. Biomaterials 2011;32:2634-41.

38. Schantz AT, Chim H, Whiteman M. P Cell Guidance in Tissue Engineering: SDF-1 Mediates Site-Directed Homing of Mesenchymal Stem Cells within Three-Dimensional Polycaprolactone Scaffolds. Tissue Eng 2007;13:2615-24.

39. Park JC. Comparative study on motility of the cultured fetal and neonatal fibroblasts in extracellular matrix. Yonsei medical journal 2011;42:587-594.

40. Park BY, Seo SW, Lee WJ, Ryu CW, Rah DK, Son HJ, et al. The Effects of Various Extracellular Matrices on Motility of Cultured MC3T3-E1 Cell. J Korean Society Plastic Recons Surgeons 2005;32:143-8.

41. Uri B, Nissim B. The tumorigenicity of human embryonic and induced pluripotent stem cells. Nature Reviews Cancer 2011;11: 268–77.

42. Nussbaum J, Minami E, Laflamme MA, Virag JAI, Ware CB, Masino A, at al. Transplantation of undifferentiated murine embryonic stem cells in the heart: teratoma formation and immune response. FASEB J 2017;21:1345-57.

II. Control of cell migration in 2-D and 3-D by fluid shear stress for tissue engineering.

1. Introduction

In tissue engineering, it is necessary that the scaffolds should be strong and have adjustable degradation time. The cells widely distributed on the scaffolds could give the appropriate mechanical strength and degradation rates to the scaffolds.[1,2] Therefore, the control of cell migration is important for inducing cell spreading and infiltration into the scaffolds.

Fluid shear stress enhances cell migration in the direction of flow and is called ‘‘mechanotaxis’’.[3] Previous studies have shown that shear stress can regulate mesenchymal stem cell (MSC) proliferation and differentiation into osteoblasts, ECs, or cardiomyocytes,[4-6] suggesting that MSCs are also sensitive to mechanical stress produced by fluid flow. Human bone marrow-derived mesenchymal stem cells (hMSCs) are ideal candidates for tissue engineering research because they are multipotent, uncommitted cells with the ability to become specialized cells and which can be relatively easily isolated.[7] They contribute to the development, regeneration and maintenance of various

mesenchymal tissues including cartilage, bone, muscle and adipose.[8-13] Many studies were accomplished to figure out the molecular mechanisms of mechanotaxis; however, it is not fully understood how the fluid shear stress regulates the directional cell migration. Cell polarization is one of the most important phenomena for the directional cell migration. Golgi apparatus (GA) polarization plays an important role in cell polarization. Golgi polarization is also significantly involved in the directional cell migration because the GA is very important in supplying the membrane components to the leading edge for membrane protrusion when the cell is moving.[14-18] Therefore, the observation of the polarization of GA induced by fluid shear stress is meaningful to understand the mechanism of mechanotaxis.

In the present study, we investigated the effect of fluid shear stress on the migration of hMSCs and figure out the enhancement of hMSCs migration into PLGA scaffold by fluid shear stress. The role of the Golgi polarization was also evaluated as a guiding cue in directional migration and infiltration of human mesenchymal stem cells (hMSCs) into electrospun poly(lactic-co-glycolic acid) (PLGA) scaffold by the fluid shear stress.

2. Materials and Methods

A. Applying the fluid shear stress to hMSCs in 2-D

Human bone marrow-derived mesenchymal stem cell (hMSCs, Lonza, Basel, Switzerland) were cultured in Mesenchymal Stem Cell Growth Medium (MSCGM, Lonza). Cells were incubated at 37 ^{o}C in a 5% CO_2 atmosphere. hMSCs between passages 5 and 9 were used in all experiments. We used the parallel plate chamber system to apply shear stress to hMSCs.[19] The parallel plate chamber system was made of incubator system installed with the microscope to observe live cells and the flow chamber to apply shear stress to the cells. The incubator was regulated by temperature and gas composition controlling program (CCP ver. 3.8) under appropriate environment for the cells (CO_2 5%, 37 ^{o}C). The flow chamber consisted of the main body, bottom plate and silicon gasket (Fig. 1A). The main body had the inlet and outlet for tubing (inner diameter, 2 mm) to apply the fluid shear stress to the cells. The hMSCs were seeded on the coverslip before mounted on the bottom plate. The main body and the silicon gasket (200 μm in height, 2 mm in width) were combined with the coverslip and bottom plate together. The medium was flowed through the inlet and outlet tube.

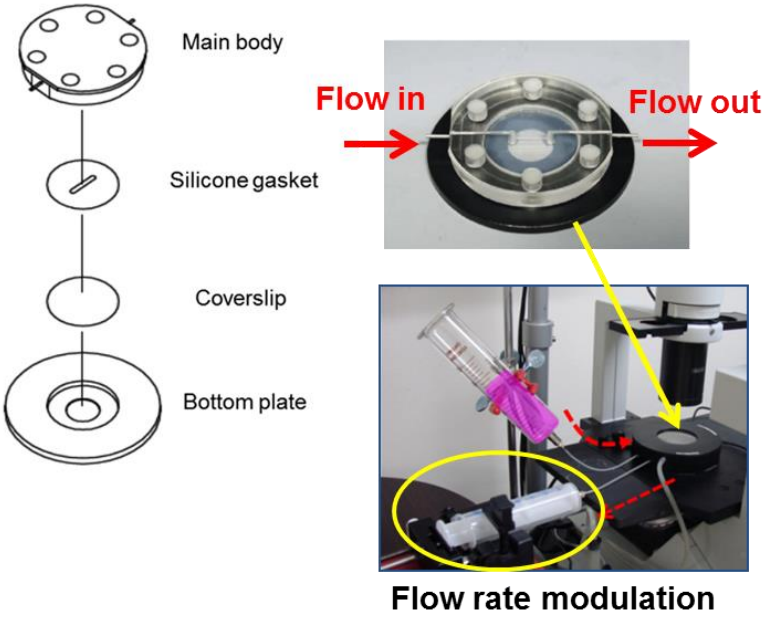

Figure. 1. The schematic of parallel plate chamber system. The main body had the inlet and outlet for tubing to apply the fluid shear stress to the cells which were seeded on the coverslip before mounted on the bottom plate.

B. Analysis of cell migration by fluid shear stress

For the migration analysis, real-time tracking system was used (Fig. 2A). The parallel plate chamber was placed on the microscope stage. The cell images were recorded every 5 min using a charge-coupled device (CCD) camera (Electric Biomedical Co. Ltd., Osaka, Japan) attached to an inverted microscope (Olympus Optical Co. Ktd., Tokyo, Japan). The images were stored to the computer by using the Tomoro image capture program; images were saved as JPEG files. Captured images were imported into ImageJ (ImageJ 1.37v by W. Rusband, National Institutes of Health, Bethesda, MD, USA). Image analysiswas carried out by the manual tracking and chemotaxis tool plug-in (v.1.01, distributed by ibidi GmbH, Munchen, Germany). The XY coordinates of each cell were obtained by using the manual tracking program. The data were imported into the chemotaxis plug-in. The cell migration speed was computed automatically and the cell migration pathway was plotted by the chemotaxis tool. The directedness of migration was assessed as cosine θ, where θ is the angle between the stimulation vector and a straight line connecting start and end positions of a cell (Fig. 2B). A cell moving directly to the down (direction of the flow) would have a directedness of 1; a cell

moving directly to the up (opposite direction of the flow) would have a directedness of -1. The value close to 0 represents the random cell movement. Therefore, an objective quantification of how directionally cells have moved was given by the average directedness of a population of cells.

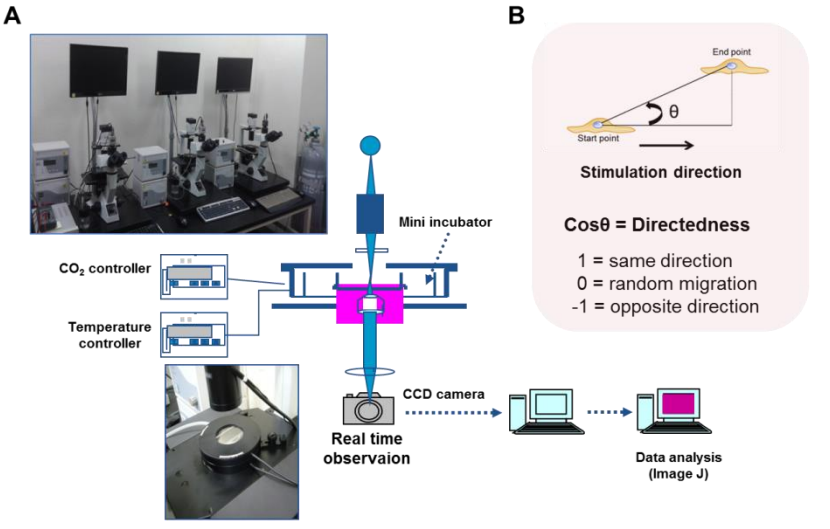

Figure. 2. Cell tracking system for migration study and definition of directedness. (A) Cell tracking system enables the real time observation of cell migration for long term because of mini incubator which is placed on the microscope connected to CCD camera. (B) The directedness of migration represent how cells moved along the direction of stimulation.

C. Electrospun PLGA scaffold

PLGA polymer (lactide/glycolide = 75:25) was purchased from Lakeshore Biomaterials (Birmingham, USA). PLGA was dissolved in a 1:4 mixture of dimethylforma-mide (DMF, Duksan Pure Chemicals co., Ltd., Ansan, Republic of Korea) and tetrahydrofuran (THF, Duksan Pure Chemicals co., Ltd., Ansan, Republic of Korea) at a concentration of 20% (w/v), and the mixture solvent was highly volatile. The polymer solution was then loaded into a syringe with 21 gauge metal needle tip. The needle tip was connected to 20 kV of a high-voltage source and a metal drum collector was served as the ground for the electrical charges. The distance between the needle tip and the drum collectorwas 10 cm, and the polymer solutionwas ejected at 2 mL/h. For the deposition of the ice crystals on the collector surface, the drum was loaded with dry ice which gives extremely low temperatures (-78.5 ^{o}C) to the drum surface. The environmental humidity was maintained at 50% approximately using a humidifier. After fabrication, the scaffolds containing ice crystals were lyophilized to maintain porous structure. The diameter of fibers was measured using the image J software program on basis of the scale bar.

D. PLGA particle containing green fluorescence fabrication

PLGA nanoparticles were prepared by an improved doubleemulsion (water-in-oil-in-water) solvent extraction technique (Fig. 3).[20] The 600 mg of PLGA (lactide/glycolide = 50:50) and 10 ml of Alexa (488)-conjugated phalloidin (Invitrogen, Carlsbad, CA) were dissolved in the dichloromethane (DCM, Duksan, Ansan, Republic of Korea). The mixed solution was vortexing for emulsion on a vortex mixer for 10 min. The emulsified solution was added gently with stirring into 50 ml of water containing 100 mg of poly(vinyl alcohol) (PVA, sigma-aldrich, St Louis, USA) to form the water-oil-water emulsion. The re-emulsified solution was poured to 50 ml of water containing 1 ml of aqueous isopropanol solution (Duksan, Ansan, Republic of Korea) then stirred for 12 h to harden the PLGA particles. After hardening, the emulsion is then subjected to solvent removal by extraction process. The emulsion was centrifused (1200 rpm, 5 min) and the supernatant was removed by suction. The solid microspheres so obtained are then washed and collected by sieving using two micro-sieves (36 μm, 50 μm). These are then dried under freeze-drier for lyophilizing to give the final microsphere product and stored at 4 ^{o}C.

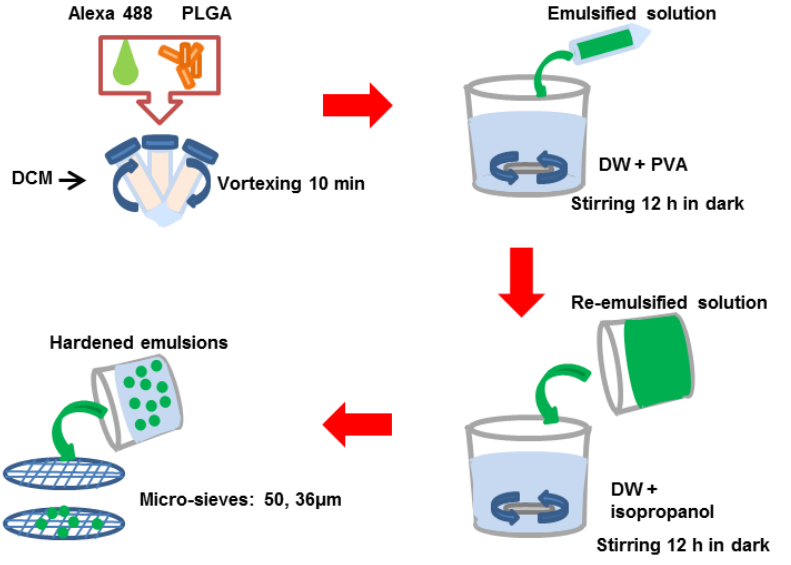

Figure. 3. Fabrication of PLGA micro particle using double emulsion method. The fabricated PLGA micro particles have green fluorescence for fluorescence microscopy observation.

E. Scanning electron microscope

The surface and the cross-sectional morphology of electrospun PLGA scaffold and distribution of PLGA particles were observed with scanning electron microscope (SEM, S-4700, Hitachi, Tokyo, Japan). The porous scaffolds and PLGA particles were coated with PT by sputtering for 3 min before SEM observation.

F. Fluid shear stress on hMSC seeded PLGA scaffold

We used the peristaltic pump to provide the fluid shear stress to the hMSCs seeded PLGA scaffold. The chamber was tapered to ensure flow from the outer edges of the scaffold as well as the center to the exit port of the chamber. The screw caps were fitted with silicon O-rings for a tight seal and prevention of leakage. The peristaltic pump pulled the medium from the reservoir and provided it to the chamber including hMSC seeded PLGA scaffold via 6 mm inner diameter silicon tubing. The culture medium was maintained at 37 ^{o}C and equilibrated with 5% CO_2 throughout the experiment. The equipment was sterilized by steam autoclave (tubing, chamber). The apparatus was assembled under sterile conditions in a laminar flow biosafety cleanbench.

G. Observation of the cells and PLGA particles in the scaffold

The cells were seeded on the PLGA scaffold (1 x 10^4 cells/scaffold, diameter of scaffold = 15 mm) and incubated in 5% CO_2 and 37 ^oC for 4 h 8 dyne/cm^2 of flow stress was applied to the cell seeded PLGA scaffold. Also, 0 and 8 dyne/cm^2 of flow stress were applied to the cells seeded PLGA scaffold with 0 and 2 μM of BFA for golgi polarization study. After 12 h applying the flow shear stress, the scaffolds were washed 3 times with PBS and the cells were fixed with pre-cooled (-20 ^oC) 70% ethanol for 15 min. The PLGA scaffold was cryosectioned, then the cells were stained with propidium iodide (Sigma, Steinheim, Germany). The infiltration of cells and PLGA particles into the scaffold were observed by a confocal microscope (LSM 700, Carl Zeiss Micro Imaging Inc., Thornwood, NY, USA).

H. Fourier transform infrared (FT-IR) spectroscopy

After 12 h applying the flow shear stress to the hMSC seeded PLGA scaffolds, the scaffolds were washed 3 times with PBS and the cells were fixed in 2.5 vol% glutaraldehyde solution at 4 ^{o}C for 1 h. After fixation, Optimal cutting temperature compound base cryo-blocks were manufactured using the fixed scaffolds, and horizontally cryo-sectioned from the surface of scaffold to 600 μm deep at intervals of 100 μm using the cryo-tome HM525 (Thermo Scientific, Hudson, NH, USA). Then, the cryo-sectioned scaffolds (thickness of each sample 100 μm) were washed 5 times with PBS and dehydrated in serial dilutions of ethanol (50, 70, 80, 90, 95, 99 and 100 vol%, respectively) for 5 min each. Dehydrated samples were freeze-dried and crushed. The crushed samples were mixed with dry KBr and pressed into a pellet using a macro KBr die kit. The solid pellet was placed in a holder and analyzed by FTIR spectrometer (Vertex 70, Bruker, Billerica, Massachusetts, USA). The spectrum was obtained with 32 scans per sample and the resolution was 4 cm^{-1}.

I. Statistical analysis

Data are reported as means ± standard error of the mean (SEM). The letter n denotes the number of tests, except in the migration assay where n denotes the number of cells. Means were compared using one-way analyses of variance (ANOVA). Two-tailed Student's t-tests were used for unpaired data. A value of $p < 0.05$ is considered statistically significant.

3. Results

A. Effects of fluid shear stress on hMSC migration

The modulation of hMSCs migration was first characterized by shear stress as a function of intensity. hMSCs were subjected to shear stress (8 dyne/cm^2, 16 dyne/cm^2) or kept as static control (0 dyne/cm^2). The migration speed and its directedness were calculated from the time-lapse microscopy (Fig. 4). Under static conditions (0 dyne/cm^2), hMSCs showed random migration without any preferential direction (Fig. 4A). The application of shear stress for 4 h, however, caused >80% (8 dyne/cm^2) or > 90% (16 dyne/cm^2) of cells to migrate in the flow direction (Fig. 4A). The effects of shear stress on the temporal change of cell migration speed (regardless of direction) are shown (Fig. 4B). After 4 h of shearing (16 dyne/cm^2), the migration speed significantly decreased by 50% above the preshear. Shear stress caused the value of directedness to increase significantly over that under static conditions (Fig. 4C). The directedness under 16 dyne/cm^2 was the highest value (0.715 ± 0.058) however the migration speed was decreased considerably. According to these results, we determined on 8 dyne/cm^2 of flow shear stress to apply to hMSCs.

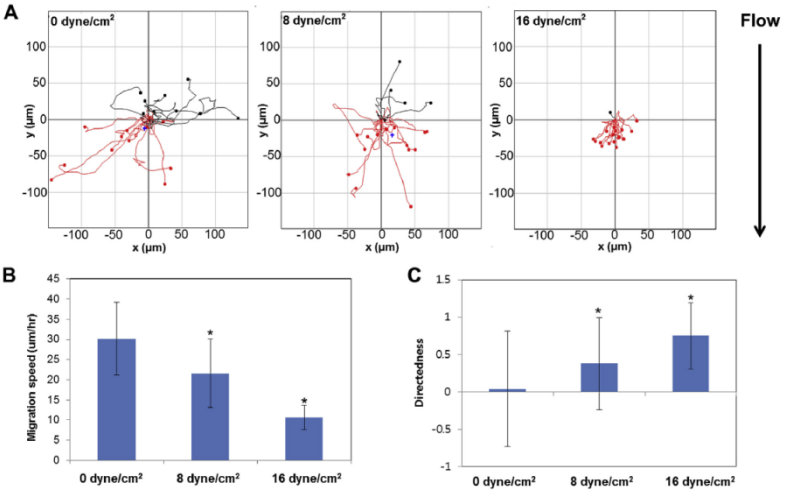

Figure. 4. The migration assay of hMSCs under flow condition (0, 8, 16 dyne/cm^2) for 4 h (A) 80 cells of each condition were tracked. (B) migration speed was measured, and (C) directedness was determined for hMSC under flow shear stress conditions for 4 h (0, 8, 16 dyne/cm^2). *$p < 0.05$ compared to controls grown with no flow shear stress (0 dyne/cm^2).

B. Inhibition of directional migration of hMSCs under fluid shear stress by blocking of Golgi polarization

To identify the effect of Golgi polarization on migration of hMSCs induced by the fluid shear stress, 0, 1, 2 and 4 μM of BFA was treated before the fluid shear stress treatment to the cells. The optimal molarity of BFA needed to be decided first for this experiment, because high concentration of BFA causes rapid dispersal of Golgi and low concentration of BFA would not affect to the Golgi. The cells showed directional migration under 8 dyne/cm^2 of fluid shear stress with 0, 1, 4 μM of BFA; however, cells moved randomly under 8 dyne/cm^2 of fluid shear stress with 2 μM of BFA (Figure 5A). The migration speed of hMSCs induced by fluid shear stress was significantly decreased when the 4 μM of BFA was treated (Figure 5B). The directedness of 0 μM was 0.452 ± 0.378; however, that of 2 μM was significantly increased and the value was 0.011 ± 0.555 (Figure 5C). These results showed that Golgi polarization of hMSCs was interrupted by 2 μM of BFA, and the directional migration of hMSCs induced by the fluid shear stress was also inhibited.

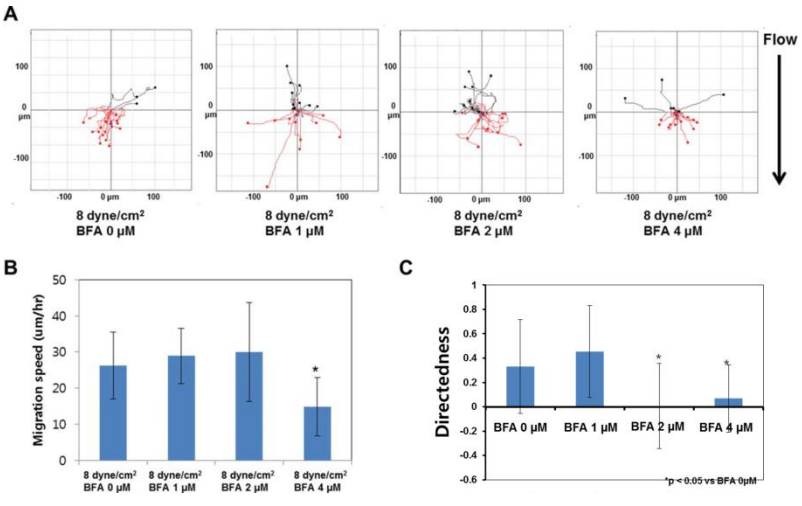

Figure. 5. The migration assay of hMSCs under flow condition (8 dyne/cm^2) for 3 h with BFA treatment (0, 1, 2, 4 μM). (A) 20 cells of each condition were tracked. (B) migration speed was measured, and (C) Directedness was determined for hMSC under flow shear stress conditions (8 dyne/cm^2) for 3 h with BFA treatment (0, 1, 2, 4 μM). *$p < 0.05$ compared to controls grown with no flow shear stress (8 dyne/cm^2 with BFA 0 μM).

C. Golgi polarization under fluid shear stress condition in 2-D

To figure out the change of cell polarization (especially Golgi polarization) by treatment 2 μM of BFA under the 8 dyne/cm^2 of fluid shear stress, the immunofluorescence images of golgi apparatus (GA) and actin cytoskeleton were observed (Figure 6A–D). In 0 dyne/cm^2 with 0 μM of BFA, the Golgi polarization and actin cytoskeleton alignment were random (Figure 6A). However, the Golgi and actin cytoskeleton were polarized toward the direction of fluid shear stress under 8 dyne/cm^2 with 0 μM of BFA (Figure 8B). There were random polarizations of Golgi and actin cytoskeleton under 0 and 8 dyne/cm^2 with 2 μM of BFA (Figure 6B,C). The Golgi dispersal and actin cytoskeleton deformations were not detected at all experimental conditions (0 and 8 dyne/cm^2 with 0 and 2 μM of BFA). To quantify the polarization of GA, we counted the polarized Golgi between 225^o and 315^o when the direction of fluid shear stress is downward (Figure 6E).[1] The quantified Golgi polarization data showed that the ratio of Golgi polarization in 8 dyne/cm^2 with 0 μM of BFA was increased significantly (Figure 8F). There were no significant changes of Golgi polarization rate under 0 and 8 dyne/cm^2 with 2 μM of BFA compared to control (0 dyne/cm^2 with 0 μM of BFA).

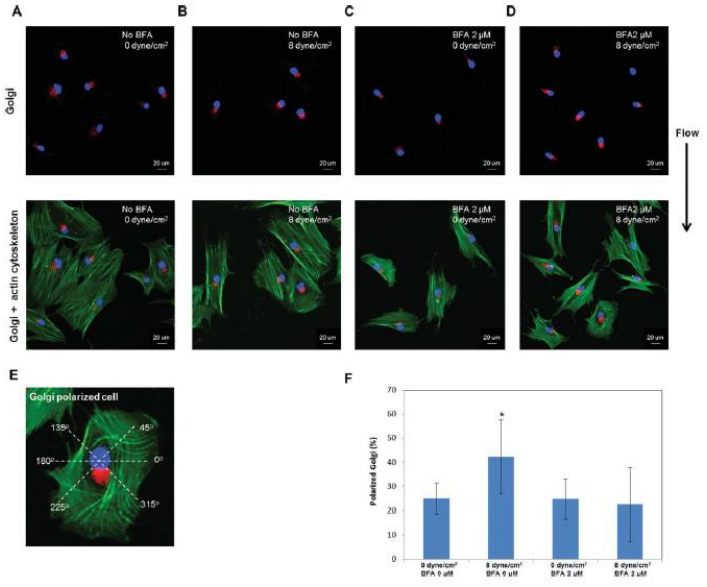

Figure. 6. Immunostaining images and Golgi polarization data of fluid shear stress and BFA treated hMSC. (A) Immunostaining of the nucleus, the actin cytoskeleton, and the GA under 0 dyne/cm^2 with no BFA, (B) 8 dyne/cm^2 with no BFA for 3 h, (C) 0 dyne/cm^2 with 2 μM of BFA for 3 h, (D) 8 dyne/cm^2 with μM of BFA for 3 h. The nuclei were stained with Hoechst, the actin cytoskeleton was stained with Alexa (488)-conjugated phalloidin (green), and GA were stained with Texas Red conjugated antibody (red). Scale bar = 20 μm. (E) GA polarization quantification is shown. (F) The percentage of cells with Golgi polarized between 225^o and 315^o. *p < 0.05 compared to the 0 dyne/cm^2 with no BFA for 3 h.

D. Low temperature electrospun PLGA (75:25) scaffold and PLGA (50:50) micro particles

The SEM images of low temperature electrospun PLGA (75:25) scaffold were shown in Fig. 3. The diameter of PLGA fibers was (1.55 ± 0.72) mm (Fig. 7A) and the thickness of the scaffold was (0.98 ± 0.14) mm. The thickness of the scaffold was measured using vernier-calipers. The edge of the low temperature scaffold could not be outlined because of its thickness (Fig. 7B). The PLGA (50:50) particles were prepared to prove that the cells infiltrated into the scaffold by mechanotaxis. The diameters of suspended hMSCs were measured to determine the appropriate size of PLGA (50:50) particles and were 37.99 ± 6.39 μm (data not shown). The SEM image of PLGA micro particles is shown in Fig. 8(A) and particle size distribution is in Fig. 8(B). The particle size distribution was measured using the Image J software program on the basis of the scale bar in SEM images.

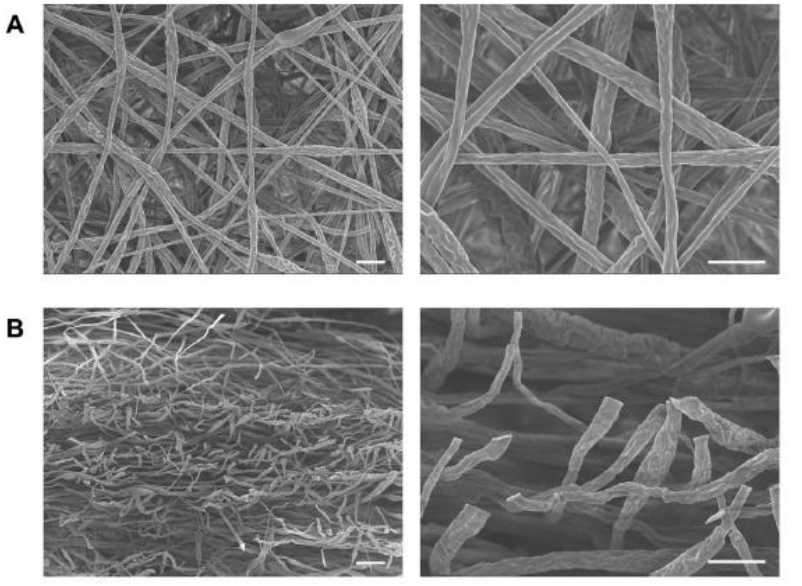

Figure. 7. Morphology of PLGA scaffold fabricated at low temperature was observed with SEM. (A) Surface of electrospun LT PLGA scaffold. (B) Cross section of electrospun LT PLGA scaffold. Scale bar = 10 μm.

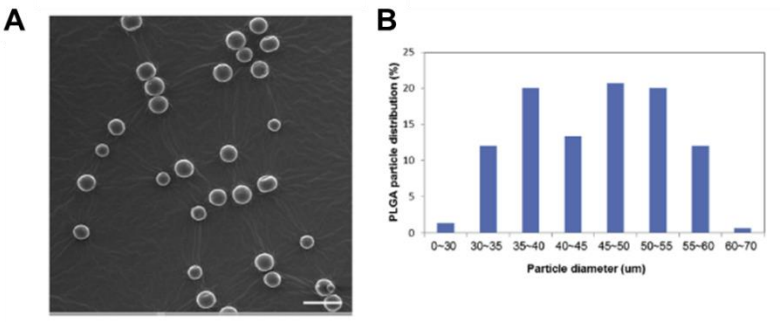

Figure. 8. Morphology of PLGA micro particles fabricated using double emulsion method were observed with SEM. (A) SEM image of the PLGA (50:50) particles. (B) Size distribution of the PLGA (50:50) particles. Number of measured particles was 150. Scale bar = 100 μm.

E. The effect of fluid shear stress on the migration of hMSC and PLGA (50:50) particles into PLGA (75:25) scaffold

To visualize hMSCs distribution inside the scaffolds after shear stress-induced cell migration cell-seeded scaffolds were stained with PI after the fixation and analyzed by confocal microscopy. Fig. 9(A) shows the cell distribution in the PLGA scaffold without flow shear stress. The cells under the flow shear stress condition (8 dyne/cm^2) migrated deeper than static conditions. The deepest distance of the cells under 8 dyne/cm^2 was 220.02 μm (Fig. 9B). The distance of infiltrated cells from the top surface of the PLGA scaffold was measured by using the Image J software program on the basis of the scale bar. mechanotaxis. The fluorescence images of PLGA (50:50) particle distribution in PLGA (75:25) scaffolds under static and fluid shear stress (8 dyne/cm^2) are shown (Fig. 9C and D).

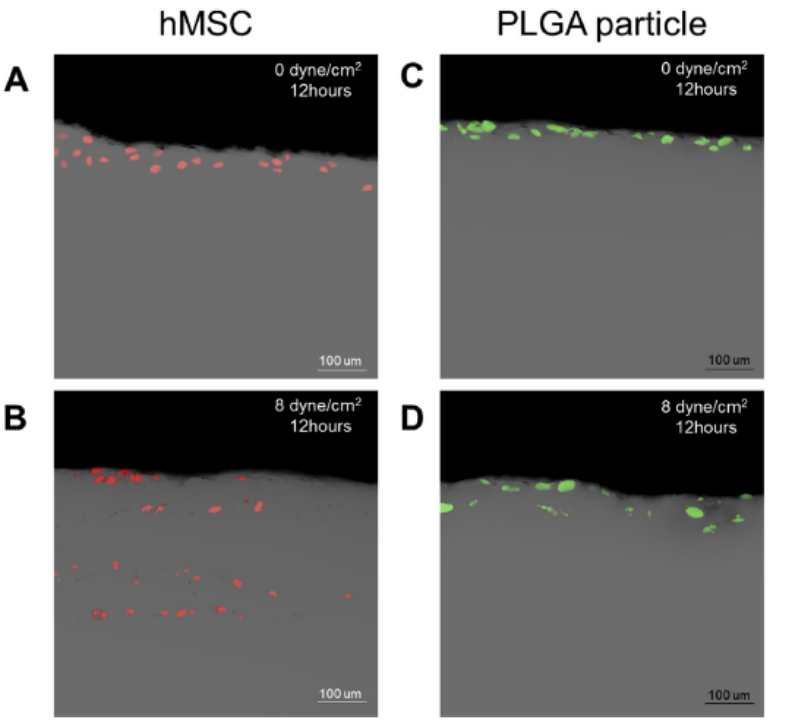

Figure. 9. The infiltration of hMSCs and PLGA particles into electrospun LT PLGA (75:25) scaffold under flow shear stress condition (0, 8 dyne/cm^2). Cross-sectional area of fluorescent image for cell distribution throughout the scaffold under (A) 0 dyne/cm^2 and (B) 8 dyne/cm2 for 12 h. Cross-sectional area of fluorescent image for the PLGA (50:50) particle distribution throughout the scaffold under (C) 0 dyne/cm^2 and (D) 8 dyne/cm^2 for 12 h. Scale bar = 100 μm.

F. Effect of Golgi polarization on migration of hMSC into PLGA scaffolds induced by fluid shear stress

To visualize the distribution of hMSCs in the PLGA scaffolds after fluid shear stressinduced cell migration, cell-seeded PLGA scaffolds were stained with PI after the fixation and analyzed by the confocal microscopy. (Figure 10A) showed the cell distribution in the PLGA scaffold under 0 dyne/cm^2 with no BFA. The deepest distance of the hMSCs under 0 dyne/cm^2 for 12 h with no BFA was 73.42 μm. The cells under the flow shear stress (8 dyne/cm^2) with no BFA condition migrated deeper than the static condition. The distance of the deepest cell was 450.82 μm under 8 dyne/cm^2 with no BFA (Figure 10B). The cells under 0 dyne/cm^2 with 2 μM of BFA showed no significant difference from 0 dyne/cm^2 with no BFA (Figure 10C). The cells under 8 dyne/cm^2 with 2 μM of BFA condition were infiltrated deeper than 0 dyne/cm^2 with 0, 2 μM of BFA. However, the cells under fluid shear stress (8 dyne/cm^2) with 2 μM of BFA condition infiltrated shallower than 8 dyne/cm^2 with 0 of BFA. The deepest distance of the cells under this condition was 184.42 μm (Figure 10D).

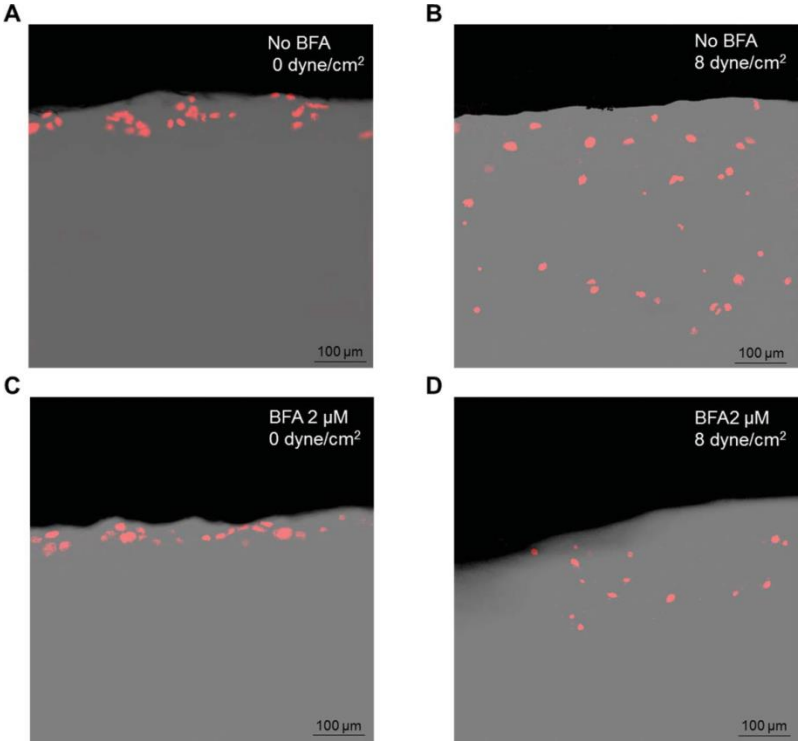

Figure. 10. The infiltration of hMSCs electrospun PLGA (75:25) scaffold under flow shear stress condition (0, 8 dyne/cm^2) with BFA (0, 2 μM). Cross-sectional area of fluorescent image for hMSCs distribution throughout the scaffold under (A) 0 dyne/cm^2 with no BFA and (B) 8 dyne/cm^2 with no BFA for 12 h. (C) 0 dyne/cm^2 with 2 μM of BFA and (D) 8 dyne/cm^2 with 2 μM of BFA for 12 h. Scale bar = 100 μm.

FT-IR spectra of three groups; hMSCs seeded PLGA scaffold with no fluid shear stress, hMSCs seeded PLGA scaffold with 8 dyne/cm^2 fluid shear stress, hMSCs seeded PLGA scaffold with 8 dyne/cm^2 fluid shear stress and 2 μM of BFA were performed. Each group was classified as 6 samples from the surface of scaffold to 600 μm deep at intervals of 100 μm, so the thickness of each sample was 100 μm. Figure 11A) shows the FT-IR spectra of the hMSCs in the PLGA scaffold under 0 dyne/cm^2 with no BFA. Amide I and amide II peaks were detected at 0~100 mm sectioned sample. When the fluid shear stress (8 dyne/cm^2) was applied to the hMSCs in PLGA scaffolds, amide I and amide II peaks were observed at 0~100 μm, 100~200 μm, 200~300 μm, 300~400 μm and 400~500 μm sectioned samples (Figure 11B). However, these two peaks were detected at 0»100 and 100~200 mm sectioned samples in the cells under the fluid shear stress (8 dyne/cm^2) with 2 μM of BFA condition (Figure 11C).

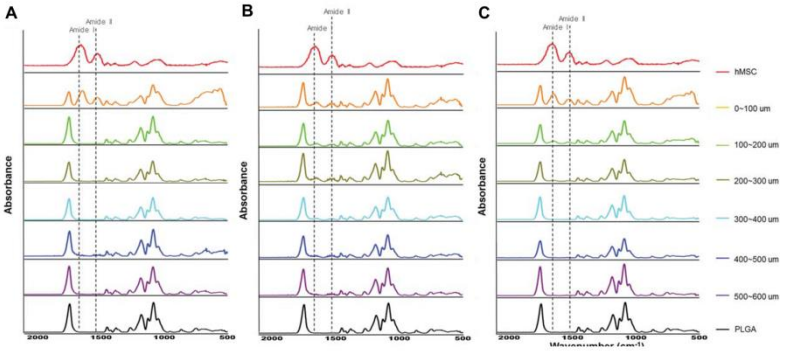

Figure. 11. FT-IR spectra of the hMSCs in the PLGA scaffolds under (A) 0 dyne/cm^2 with no BFA and (B) 8 dyne/cm^2 with no BFA for 12 h. (C) 8 dyne/cm^2 with 2 μM of BFA for 12 h.

4. Discussion

Mechanical forces are known to be important in a variety of cellular processes, actively participating in the regulation of cell growth, differentiation, gene expression and migration.[21] Cells are able to detect and respond to shear stress through mechanotransduction, a complex process that converts mechanical forces into biochemical signals and integrates these into a cellular response.[22]

A wide array of architectural configurations and geometries can be created using scaffold fabrication technologies such as rapid prototyping, melt extrusion, salt leaching, emulsion templating, phase separation, and electrospinning.[23] The electrospinning was chosen to fabricate the scaffold because electrospining is a process that can generate fiber mesh scaffolds with high porosities, large surface area-to-volume ratios, and variable fiber diameters.[24,25] These features, along with the versatility and simplicity of the system, make electrospinning an attractive tool for the production of scaffolds.

Cells were able to detect and respond to the fluid shear stress through the mechanotransduction, a complex process that converts

mechanical forces into biochemical signals and integrates these into a cellular response.[26] Polarization of GA plays an important role in directional cell migration.[16] BFA prevents the assembly of cytosolic coat proteins onto Golgi membranes, resulting in the formation of Golgi tubules and prevents tubule detachment from the Golgi structure which then fuses with the endoplasmic reticulum (ER). This leads to diffusion of Golgi membrane into the ER and disruption of Golgi. BFA at high concentrations of 2–5 mg/mL (~18 mM) causes this rapid dispersal of the Golgi within 5–8 min after addition of the BFA.[26-28] 5 μM of BFA induced quick dispersal of the GA. This treatment resulted in discoid cell morphology.[14] It is impossible to analyze Golgi polarization and cell migration if there is no visible Golgi staining or the cells do not move. The purpose of this experiment was determination of BFA concentration which is blocking the Golgi polarization of cells but is not affecting to the migration speed induced by 8 dyne/cm^2 fluid shear stress. The blocking of Golgi polarization could be inferred indirectly from losing the directional migration. In our previous study, the optimal condition of hMSCs directional migration by the fluid shear stress (8 dyne/cm^2) was decided,[29] and we identified the reproducibility that the cells moved along the fluid shear stress in this study. The migration speed was not

changed and direction of cell migration was same as the fluid shear stress in 1 μM of BFA treatment, so the effect of BFA was not expected. In 4 μM of BFA, that concentration of BFA could not be used since the migration speed was significantly decreased. The migration speed was not changed and directional migration was interrupted in 2 μM of BFA, thus this concentration was selected as an optimal molarity of this experiment. The directional migration of Chinese hamster ovary cell and neonatal human dermal fibroblast induced by electric stimulation was inhibited by 1 μM of BFA;[14,30] however, directional migration of hMSCs induced by fluid shear stress was interrupted by 2 μM of BFA. According to these results, the appropriate molarity of BFA which induce the Golgi blocking was specific to the cell types or experimental condition, and also Golgi polarization plays an important role in directional migration induced by fluid shear stress.

The FT-IR scans of the hMSCs, PLGA scaffolds and hMSC seeded PLGA scaffolds were analyzed to evaluate the infiltration of cells into the PLGA scaffolds. The FT-IR spectra of hMSCs and PLGA scaffolds were inspected before the screening of hMSC seeded PLGA scaffold (data not shown). Several FT-IR peaks attributing to the presence of amide I at 1670 cm^{-1}, amide II at 1540 cm^{-1},

water at 3350 cm^{-1} and C–H at 2970 cm^{-1} were detected for hMSCs.[31-34] However, typical bands for ester carbonyl stretch (CDO) at 1745 cm^{-1}, C–O stretch at 1173 cm^{-1} and C–O–C group at 1083 cm^{-1} were found for PLGA scaffolds.[35] Amide I and amide II peaks were not observed for the PLGA scaffolds, so these peaks indicated the presence of hMSCs in the PLGA scaffolds.

Contrary to the general cell migration in 2D, active and directional migration was required in 3D cell infiltration because cell infiltration was interrupted by the structure of 3D scaffolds. Many studies about enhancing the infiltration into 3D scaffolds have been progressing in tissue engineering area. We used fluid shear stress to induce the cell migration into the inside of scaffolds, as a result the promotion of infiltration by fluid shear stress was suceeded.[29] However, the reason of infiltration improvement was still needed to be figured out. It could be a just mechanical force of fluid shear stress or a change of active migration by mechanotransduction.

Fig. 9A and B suggest that flow shear stress enhances the infiltration of hMSCs into PLGA scaffold, however the reason that infiltration of hMSCs enhanced by flow shear stress still needs to be figured out either cells were pushed by mechanical force of flow shear stress or migrated into the scaffold actively by mechanotaxis.

In Fig. 9C and D, it is obvious that there is no significant differences of particle infiltration into scaffolds between static condition and fluid shear stress applied condition. These results support that hMSCs were not just pushed to the inside of scaffolds by physical force of fluid shear stress. Identifying the actual mechanism for mechanotaxis of hMSCs would constitute a major step towards verifying this hypothesis. Figure 5 and 6 showed that 2 μM of BFA blocked Golgi polarization induced by fluid shear stress and inhibit the directional migration. Other study suggested that hMSCs infiltration into PLGA scaffold was increased by 8 dyne/cm^2 of fluid shear stress but PLGA microparticle infiltration was not changed by 8 dyne/cm^2 of fluid shear stress.[29] In Figure 10, the infiltration of hMSCs into PLGA scaffold by fluid shear stress was decreased by the inhibition of Golgi polarization. According to these results fluid shear stress enhanced the infiltration of hMSCs into PLGA scaffold, and active migration caused by mechanotransduction was concerned with it. Golgi polarization also affected to the infiltration of hMSCs into PLGA scaffold induced by fluid shear stress. The infiltration of cells into PLGA scaffold by fluid shear stress was analyzed by spectroscopy method (Figure 11). SEM and immunofluorescence were mainly used to analyze the cell infiltration into scaffold as an established method

however those two methods have some limitations. In SEM analysis, the surface of cross-sectioned sample should be flat and even, and the structure of scaffold needed to be maintained when the sample was cross-sectioning. In immunofluorescence analysis, the determination of appropriate concentration of fluorescence antibody was preceded, and those concentrations depended on the cell type or variety of scaffolds. The immunofluorescence image shows only the surface of cross-sectioned sample, so a lot of immunofluorescence images were required to figure out the cell population in whole scaffold. However, FT-IR made the whole scaffold screening possible and sample preparation ease. The immunofluorescence data (Figure 10) and FT-IR data (Figure 11) were almost matched so these results suggest that the inhibition of Golgi polarization affected the infiltration of hMSCs into the PLGA scaffold under fluid shear stress condition. Also, the induction of Golgi polarization is necessary to induce the directional migration and enhancement of infiltration using the fluid shear stress.

5. Conclusion

In summary, this study showed that the fluid shear stress enhanced the migration of hMSCs into PLGA scaffold and the Golgi polarization affected mechanotaxis. The cells moved along the direction of flow and they were also infiltrated into the PLGA scaffold by the fluid shear stress. However, the infiltration of PLGA micro particles into PLGA scaffolds was not affected by the fluid shear stress. The directional migration of the cells along the direction of flow was inhibited by treatment 2 μM of BFA and the infiltration into the PLGA scaffold was affected too. These results suggest that the cells were migrated into the PLGA scaffold by responding to the fluid shear stress through the mechanotransduction. Also the Golgi polarization plays an important role in the directional migration and enhancement of migration of hMSCs by responding to the fluid shear stress. The enhancement of hMSCs migration into PLGA scaffold through fluid shear stress could be an important technique for promoting the cell distribution into scaffolds homogeneously for tissue engineering.

References

1. Kim MS, Lee MH, Kwon, BJ, Park JC. Control of neonatal human dermal fibroblast migration on poly (lactic-co-glycolic acid)-coated surfaces by electrotaxis. J Tissue Eng Regen Med 2017;11:862-8.

2. Ma Z, Gao C, Gog Y, Shen T. Cartilage tissue engineering PLLA scaffold with surface immobilized collagen and basic fibroblast growth factor. Biomaterials 2005;26:1253-9.

3. Song L, Peter B, Yingxiao W, Yingli H, Shunichi H. The role of the dynamics of focal adhesion kinase in the mechanotaxis of endothelial cells. Proc Natl Acad Sci U S A 2009;99:3546-51.

4. Tu ML, Wang HQ, Sun XD, Chen LJ, Ke ZJ, Pim-1 is upregulated by shear stress and is involved in shear stressinduced proliferation of rat mesenchymal stem cells. Life Sci 2011;88:233-8.

5. Yourek G, McCormick SM, Mao JJ, Reilly GC. Shear

stress induces osteogenic differentiation of human mesenchymal stem cells. Regen Med 2010;5:713-24.

6. Huang Y, Jia X, Bai K, Gong X, Fan Y. Effect of fluid shear stress on cardiomyogenic differentiation of rat bone marrow mesenchymal stem cells. Arch Med Res 2010;41: 497-505.

7. Pittenger MF, Mackay AM, Beck SC, Jaiswal RK, Marshak DR. Multilineage potential of adult human mesenchymal stem cells. Science 1999;284:143-7.

8. Bruder SP, Fink DJ, Caplan AI. Mesenchymal stem cells in bone development, bone repair and skeletal regeneration therapy. J Cell Biochem 1994;56:283-94.

9. Prockop DJ. Marrow stromal cells as stem cells for nonhematopoietic tissues. Science 1997;276:71-4.

10. Bab I, Howlett CR, Ashton BA, Owen ME. Ultrastructure of bone and cartilage formed in vivo in diffusion chambers. Clin Orthop Relat Res 1984;187:243-54.

11. Friedenstein AJ, Chailakhyan RK, Gerasimov UV. Bone marrow osteogenic stem cells: in vitro cultivation and

transplantation in diffusion chambers. Cell Tissue Kinet 1987;20:263-72.

12. Mardon HJ, Bee J, Mark K, Owen ME. Development of osteogenic tissue in diffusion chambers from early precursor cells in bone marrow of adult rats. Cell Tissue Res 1987;250:157-65.

13. Caplan AI, Mesenchymal stem cells. Orthop Res 1991;9:641-50.

14. Kim MS, Lee MH, Kwon BJ, Park JC. Golgi polarization plays a role in the directional migration of neonatal dermal fibroblasts induced by the direct current electric fields. Biochem Bioph Res Co 2015;460:255-60.

15. Raftopoulou M, Hall A. Cell migration: Rho GTPases lead the way. Dev Biol 2004;265:23-32.

16. Bershadsky AD, Futerman AH. Disruption of the Golgi apparatus by brefeldin A blocks cell polarization and inhibits directed cell migration. Proc Natl Acad Sci U S A 1994;91:5686-9.

17. Nabi IR. The polarization of the motile cell. J Cell Sci

1999;112:1803-11.

18. Prigozhina NL, Waterman-Storer CM. Protein kinase Dmediated anterograde membrane trafficking is required for fibroblast motility. Curr Biol 2004;14:88-98.

19. Koo MA, Kang JK, Lee MH, Seo HJ, Kwon BJ, You KE, et al. Stimulated migration and penetration of vascular endothelial cells into poly (l-lactic acid) scaffold under flow conditions. Biomaterials Res 2014;18:48-54.

20. Liu J, Zhang SM, Chen PP, Cheng L, Ke CM. Controlled release of insulin from PLGA nanoparticles embedded within PVA hydrogels. J Mater Sci Mater Med 2007;18:2205-10.

21. Katsumi A, Orr W, Tzima E, Schwartz MA. Integrins in mechanotransduction. J Biol Chem 2004;279: 12001-4.

22. Huang H, Kamm RD, Lee RT. Cell mechanics and mechanotransduction:pathways, probes, and physiology. J Physiol Cell Physiol 2004;287:C1-11.

23. Quynh PP, Upma S, Mikos AG. Electrospun Poly(E-caprolactone) microfiber and multilayer

nanofiber/microfiber scaffolds: characterization of scaffolds and measurement of cellular infiltration. Biomacromolecules 2006;7:2796-805.

24. Wnek GE, Carr ME, Simpson DH, Bowlin GL. Electrospinning of nanofiber fibrinogen structures. Nano Lett 2003;3:213-6.

25. Subbiah T, Bhat GS, Tock RW, Pararneswaran S, Ramkumar S. Electrospinning of nanofibers. J Appl Polym Sci 2005;96:557-69.

26. Presley JF, Smith C, Hirschberg K, Miller C, Cole NB, Lippincott-Schwartz J. Golgi membrane dynamics. Mol Biol Cell 1998;9:1617-26.

27. Sciaky N, Presley J, Smith C, Zaal KJM, Lippincott-Schwartz J. Golgi tubule traffic and the effects of brefeldin A visualized in living cells. J Cell Biol 1997;139:1137-55.

28. Hirschberg K, Miller CM, Ellenberg J, Presley JF, Lippincott-Schwartz J. Kinetic analysis of secretory protein traffic and characterization of Golgi to plasma membrane transport intermediates in living cells. J Cell Biol 1998;143:1485-503.

29. Kim MS, Lee MH, Kwon BJ, Park JC. Enhancement of human mesenchymal stem cell infiltration into the electrospun poly(lactic-co-glycolic acid) scaffold by fluid shear stress. Biochem Bioph Res Co 2015;463:137-42.

30. Pu, J, Zhao M. Golgi polarization in a strong electric field. J Cell Sci 2005;118:1117-28.

31. Shetty G, Kedall C, Shepherd N, Stone N, Barr H. Raman spectroscopy:evaluation of biochemical changes in carcinogenesis of oesophagus. Br J Cancer 2006;94:1460–1464.

32. Gazi E, Dwyer J, Gardner P, Ghanbari-Siakhani A, Wde A P, Lockyer NP, et al. Applications of Fourier transform infrared microspectroscopy in studies of benign prostate and prostate cancer. J Pathol 2003;201:99-108.

33. Paluszkiewicz C, Kwiatek WM. Analysis of human cancer prostate tissues using FTIR microscopy and SXIXE techniques. J Mol Struct 2001;565-566:329-334.

34. Dovbeshko GI, Chegel VI, Gridina NY, Repnytska OP, Shirshov YM, Tryndiak VP, et al. Surface enhanced IR absorption of nucleic acids from tumor cells: FTIR

reflectance study. Biopolymers 2002;67:470-86.

35. Jose MV, Thomas V, Dean DR, Nyairo E. Fabrication and characterization of aligned nanofibrous PLGA/Collagen blends as bone tissue scaffolds. Polymer 2009;50:3778-85.

III. Control of cell migration in 2-D and 3-D by electric stimulation for tissue engineering.

1. Introduction

Cell migration is essential to tissue regeneration and morphogenesis. Cell movement can be controlled by chemical cues and by physiological electric fields (EFs), which are established by a transepithelial potential difference in tissues that provides directional and morphogenic cues during embryonic development, morphogenesis, wound healing, neurogenesis and neuroregeneration.[1-6]

Applied direct current electric fields (dc EFs) guide the directional migration of many cell types, including endothelial cells, bone marrow mesenchymal stem cells and human dermal fibroblasts.[7-9] The dc EFs also induced the directional cell migration in wound healing and development in vivo.[10-16] We refer to this as "electrotaxis/galvanotaxis." During electrotaxis, cells move toward the anode or cathode under direct current electric fields (dc EFs); these dc EFs can be used to control the directional cell migration. In addition, the dc EFs may have in vivo or in vitro application of the technique to induce the predictable cell polarization and directional cell migration. Our previous research already confirmed

that the change of Golgi apparatus polarization and cytoskeleton reorganization during the directional migration by the dc EFs.[17]

In tissue engineering, it is essential that scaffolds be strong and have adjustable degradation rates. Cells that are widely distributed on scaffolds can aid in mechanical strength and degradation rates.[18] Control of cell migration, however, is important for inducing cell spreading and infiltration into the scaffolds. This study was designed to figure out the role of Golgi polarization as a predominant guidance cue in directed cell migration by dc EFs.

In the present study, we investigated the effect of electric stimulation on the migration of nHDF and hMSCs and figure out the enhancement of hMSCs migration into PCL scaffold by electric stimulation. The role of the Golgi polarization was also evaluated as a guiding cue in electrotaxis and migration of human mesenchymal stem cells (hMSCs) into 3D printed PCL scaffold by the electrotaxis.

2. Materials and Methods

A. Chemical agents and cell culture

Brefeldin A (BFA) was from Sigma (St. Louis, MO, USA). Neonatal human dermal fibroblasts (nHDFs) were purchased from Lonza Group, Ltd. (Walkersville, MD, USA) and maintained in fibroblast basal medium-2 (FBM-2) supplemented with a growth kit containing 10 ml of fetal bovine serum, 0.5 ml of insulin, 0.5 ml of gentamicin sulfate amphotericin-B (GA-1000), and 0.5 ml of r-human fibroblast growth factor-B (Lonza, USA). Human mesenchymal stem cells (hMSC, Lonza, Basel, Switzerland) were cultured in mesenchymal stem cell growth medium (MSCGM, Lonza). The cells were incubated at 37 ^{o}C in a 5% CO_2 atmosphere. nHDFs between passages 7 and 9 , hMSCs between 3 and 5 were used in all experiments.

B. Electric stimulation and drug treatment

To apply a direct current electric field to the nHDFs, we used a customized electrotaxis incubator and chamber system.[17] Briefly, the electrotaxis chamber and incubator system consisted of the incubator system and electrotaxis chamber. The incubator system is installed with a microscope to observe live cells and the electrotaxis chamber applies a direct current electric field to the cells. A gold patterned glass slide was mounted on the chamber bottom, and the chamber top and silicon gasket were placed on top of the slide. The electrotaxis chamber top with the electric wires connects the gold patterned. To sterilize the chamber, 70% ethanol (700 μl) was added to each electrotaxis chamber and removed after 30 min followed by three washes with distilled water (DW). The nHDFs were seeded at 1 x 10^4 cells density in the electrotaxis chamber and incubated for 16-24 h in the CO_2 incubator. Immediately before electrotaxis experiments, media was changed. Cells were exposed to a dc EF at 37 ^oC in the electrotaxis incubator and chamber system.1 μM of BFA was treated to interrupt the Golgi polarization before or during the dc EF stimulation

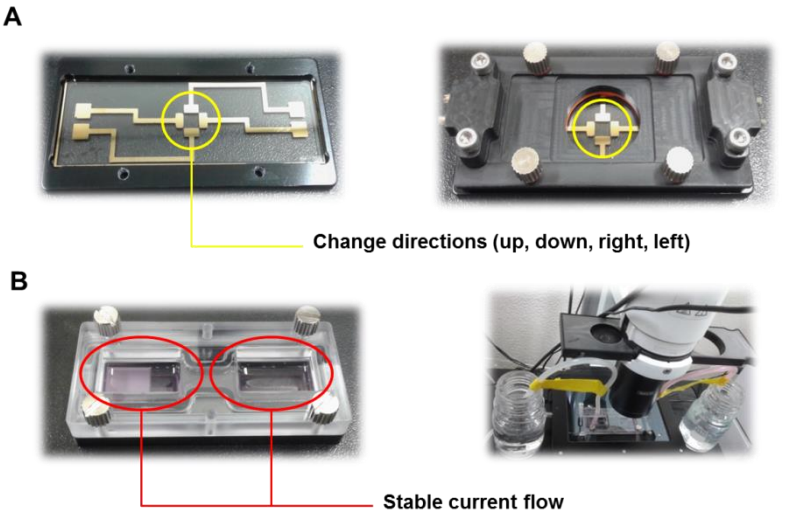

Figure. 12. Electric stimulation treatment system. (A) Gold-patterned slide glass used to control the direction of the current. (B) Customized agar-salt electrotaxis chamber.

C. Immunofluorescence microscopy

After electric current treatments, nuclei, GA and actin cytoskeletons were visualized by immunofluorescence staining. The dc EF treated cells were fixed with 70% ethanol for 30 min at 4 ^{o}C and were then washed 3 times with PBS. Cells were permeabilized with 0.1% Triton X-100 in PBS for 5 min at room temperature and rinsed 3 times with PBS. 1% Bovine serum albumin (BSA) was treated for 30 min at room temperature to block the nonspecific binding with, followed by incubation with a purified mouse anti-GM130 primary antibody (dilution 1:100, BD Transduction Laboratories TM, BD Biosciences, CA, USA) overnight at 4 C. Cells were then washed at least 3 times with PBS and treated with the secondary antibody Alexa (488)-conjugated phalloidin (5 U/ml, Invitrogen, Carlsbad, CA) for the actin cytoskeleton and goat anti-mouse IgG conjugated with Texas Red (dilution 1:100, Santa Cruz, CA, USA) for the GA, for 1 h at room temperature in the dark. After PBS washing, cells were treated with Hoechst #33258 (Sigma, St. Louis, MO, USA) for 5 min at room temperature in the dark. The cell seeded slide glass was then mounted on the fluorescence-inverted microscope (LSM700, Carl Zeiss, New York, USA) and observed.

D. Golgi polarization analysis

The nHDF cells in a dc EF of 1 V/cm for 2-5 h showed distinct polarized morphology and Golgi apparatus. The cells with the polarized Golgi between 45^{o} and 315^{o} (cathode right) or between 135^{o} and 225^{o} (cathode left) of the dc EF direction were scored as polarized in the EF direction.

E. In vivo implantation studies

All animal experiments were performed in accordance with the "Guide for the Care and Use of Laboratory Animals." The Institutional Animal Care and Use Committee of the Yonsei Laboratory Animal Research Center (YLARC) approved all protocols (Permit #: 2017-0245). Nine Balb/c nude mice (male, 6 weeks, Orient bio, Korea) were anaesthetized and two approximately 8 mm dorsal incisions were made on each mouse to create subcutaneous pockets. The PCL scaffolds were transferred into the both side of separate pockets of 3 mice. The hMSC seeded PCL scaffolds were implanted into left of pockets and electric stimulation treated-hMSC seeded PCL scaffolds were implanted into right of pockets of 5 mice, then the skin was closed using Vicryl 5.0 sutures. The mice were maintained in a pathogen-free facility at the YLARC. After 1, 2 and 3 weeks, the animals were sacrificed, and the scaffolds were obtained for histological examination.

F. Histological examination

The retrieved scaffolds (n = 2 per scaffold per time point) together with the ingrown tissues were fixed in formalin. The fixed implants were dehydrated through a graded series of alcohol solutions and then transferred into xylene. This procedure resulted in dissolution of the remaining scaffolds present in the tissue. The fixed tissues were subsequently embedded in paraffin. The obtained paraffin blocks were then cut into 5 μm thick sections, deparaffinizied in xylene and rehydrated in graded series of alcohol prior to staining. The sections were stained with hematoxylin and eosin (H & E) for microscopic examination.

G. Statistical analysis

Data are reported as means ± standard error of the mean (SEM). The letter n denotes the number of tests, except in the migration assay where n denotes the number of cells. Means were compared using one-way analyses of variance (ANOVA). Two-tailed Student's t-tests were used for unpaired data. A value of $p < 0.05$ is considered statistically significant.

3. Results

A. Blocking of Golgi polarization inhibited the directional migration induced by the dc EF

In our previous study, the optimal condition of nHDFs directional migration by the electrotaxis was identified and the Golgi polarization was observed during the electrotaxis. The cell moved randomly without EF, and cell migrated toward the cathode under the dc EF 1 V/cm for 2 h (Fig. 13A). However, there was no directional migration when the BFA was treated before the 1 V/cm EF stimulation. The migration speed of nHDFs was not affected by both dc EF and BFA treatment (Fig. 13B). The directdness of 0 V/cm and 1 V/cm BFA were closed to “0”, however that of 1 V/cm was significantly increased (Fig. 13C). These results indicated that the interruption of Golgi polarization inhibits the directional migration of nHDF induced by the dc EF.

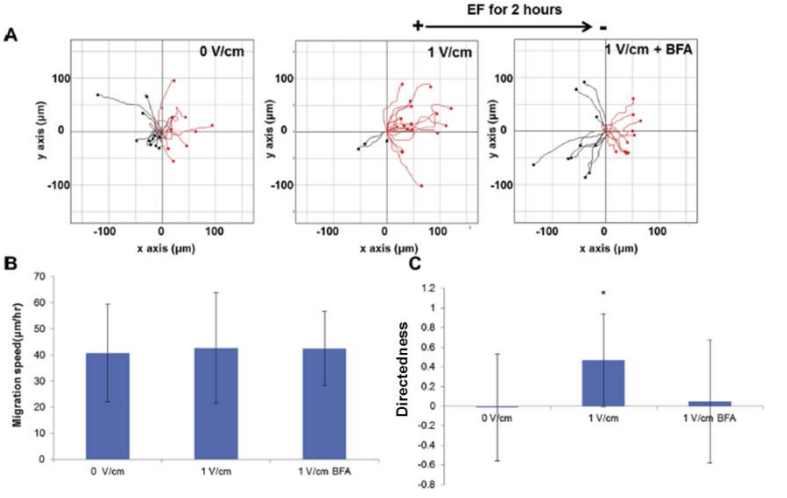

Figure. 13. The migration assay of nHDFs under dc EF condition (0, 1 V/cm) for 2 h with or without 1 mM of BFA. (A) 20 Cells of each condition were tracked, (B) migration speed was measured, and (C) directedness was determined for nHDFs under dc EF conditions for 2 h (0, 1 V/cm), *p < 0.05 compared to controls grown with no EF.

B. Golgi polarization versus Golgi dispersal in dc EF

To figure out the optimal condition of BFA and dc EF treatment, first the cells were polarized toward the cathode by the 1 V/cm EF for 2 h. Then the 1 μM of BFA was treated immediately and dc EF stimulation was stopped. The immunofluorescence images of Golgi apparatus and actin cytoskeleton were observed (Fig. 14A-D). In no dc EF condition, the Golgi and actin cytoskeleton polarization were random (Fig. 14A). However, the Golgi and actin cytoskeleton were polarized toward the cathode under 1 V/cm EF for 2 h without BFA (Fig. 14B). There were no significant changes of polarized Golgi after BFA treatment for 2 h. The Golgi polarization was still toward cathode and deformation of actin cytoskeleton was not observed (Fig. 14C). The Golgi dispersal and actin cytoskeleton deformations were detected at 3 h after BFA treatment (Fig. 14D). The white arrows indicated the Golgi dispersal and round shaped actin cytoskeleton. The quantified Golgi polarization data showed that the percent of Golgi polarization in 1 V/cm 2 h and 1 V/cm 2 h with BFA 2 h were increased significantly, but slightly decreased in 1 V/cm 2 h þ BFA 3 h (Fig. 14F). The drop of Golgi polarization in 1 V/cm 2 h þ BFA 3 h was due to the dispersal of Golgi apparatus by BFA effect.

According to these results, 2 h after 1 μM of BFA treatment is optimal condition for the experiment that BFA could cause the derangement of Golgi complex reorientation, although did not cause complete dispersal of Golgi.

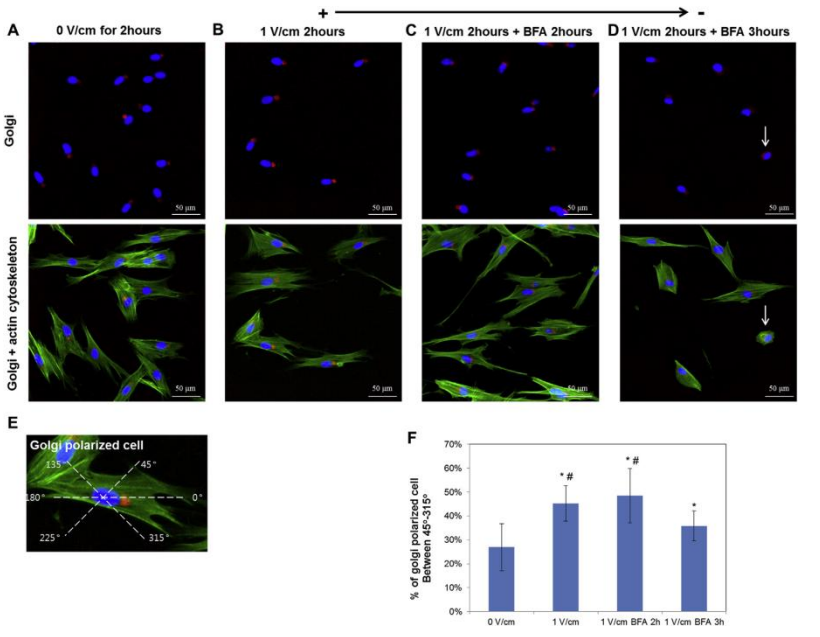

Figure. 14. Immunostaining images and Golgi polarization data of dc EF and BFA treated nHDFs. (A) Immunostaining of the nucleus, the actin cytoskeleton, and the GA under 0 V/cm, (B) 1 V/cm for 2 h, (C) 1 V/cm for 2 h then 1 mM of BFA treated for 2 h, (D) 1 V/cm for 2 h then 1 mM of BFA treated for 3 h. The nuclei were stained with Hoechst, the actin cytoskeleton was stained with Alexa (488)-conjugated phalloidin (green), and GA were stained with Texas Red (red). Scale bar = 50 mm. (E) GA polarization quantification is shown. (F) The percentage of cells with Golgi polarized between 45^{o} and 315^{o}. *$p < 0.05$ compared to the 0 V/cm and #$p < 0.05$ compared to the 1 V/cm BFA 3 h.

C. Golgi polarization is more important to the directional migration than the dc EF

To identify the effect of Golgi polarization on the dc EF induced directional migration, 1 μM of BFA was treated immediately after the cells were exposed to 1 V/cm dc EF for 2 h. The direction of dc EF was reversed right after the BFA treatment and maintained the direction of reversed dc EF for another 2 h. The cells in no dc EF showed random migration for 2 h and 4 h (Fig. 15A and B). When the cathode was right, the cells also moved toward right (Fig. 15C and E). The cells moved toward right for first 2 h and the direction of cell migration was changed toward left response to the switch in the direction of the dc EF toward left (Fig. 15D). However, the cells treated with BFA after dc EF induced directional migration toward right maintained the direction of migration toward right even though the dc EF was reversed (Fig. 15F). The directedness of 0 V/cm were closed to “0” from 1 h to 4 h. The directedness of 1 V/cm significantly increased until 2 h, after that it considerably decreased because the direction of dc EF was reversed. However, that of 1 V/cm + BFA at 2 h increased remarkably and kept the high value of directedness (Fig. 16).

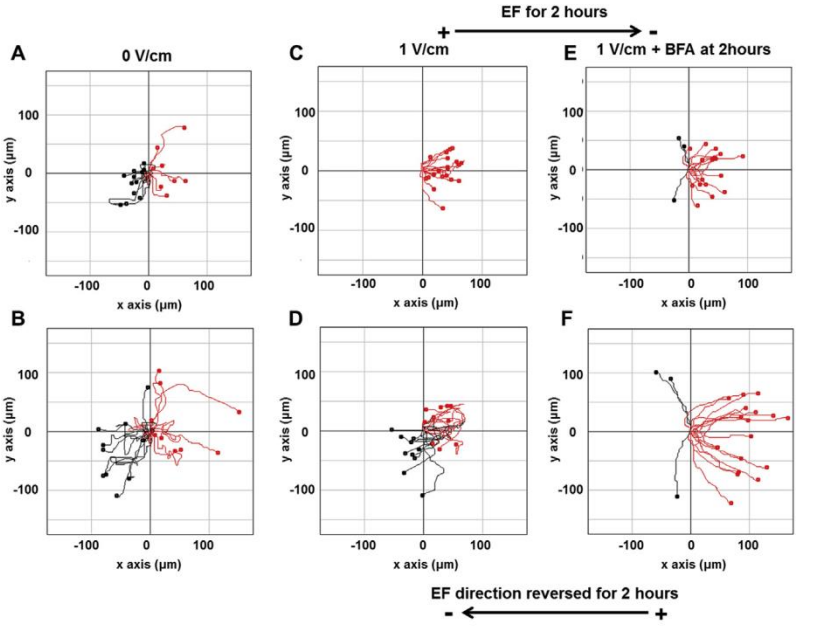

Figure. 15. The cell tracking data of nHDFs in an EF. The movement of cells for 2 h (A) and 4 h (B) in no dc EF. The direction of dc EF was right (cathode right) for 2 h (C) then reversed the direction for 2 h (D). (E) Cell tracking data that the direction of dc EF was right for 2 h. (F) 1 μM of BFA treated immediately before reverse the direction for 2 h.

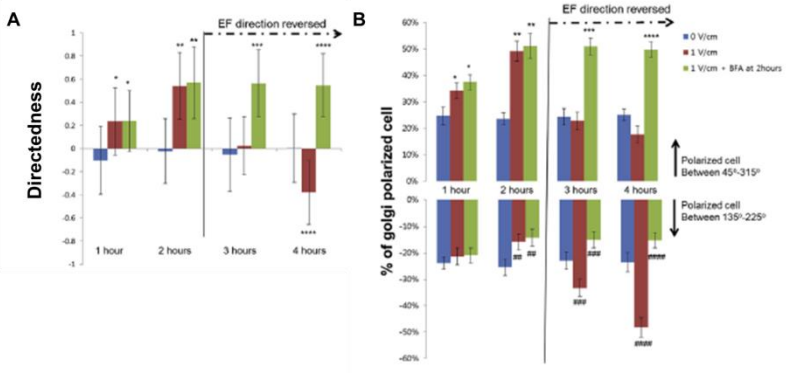

Figure. 16. The Golgi polarization data of nHDFs in an EF. (A) Directedness determined for nHDFs under dc EF conditions for 4 h (0, 1 V/cm). *p < 0.05 compared to directedness of EF 0 V/cm at 1 h, **p < 0.05 (0 V/cm at 2 h), ***p < 0.05 (0 V/cm at 3 h), ****p < 0.05 (0 V/cm at 4 h). (B) The percentage of cells with Golgi polarized between 45^{o} and 315^{o}, between 135^{o} and 225^{o}. *p < 0.05 compared to the polarized cell between 45^{o} and 315^{o} EF 0 V/cm at 1 h, **p < 0.05 (1 V/cm at 2 h), ***p < 0.05 (1 V/cm), ****p < 0.05 (1 V/cm at 4 h). ##p < 0.05 compared to the polarized cell between 135^{o} and 225^{o} EF 1 V/cm at 2 h, ###p < 0.05 (1 V/cm at 3 h), ####p < 0.05 (1 V/cm at 4 h).

D. Migration of hMSCs by electrotaxis in 2-D

In gold pattern system, the current flow was not stable. The early current maintained short time then decreased (Fig. 17), so we used agar system to stable the current flow. We added media reservoir and cell seeded and observed to that area. The current is stable and real time migration observervation was possible (Fig. 17).

To study the migration control about stem cells, we treated various electric current using the agar system to find the optimal condition (Fig. 18A). The migration speed was not affected by electric current (Fig. 18B) but, the directedness was significantly increased from 1000 μA (Fig. 18C). So we choose the 1000uA for hMSC electrotaxis.

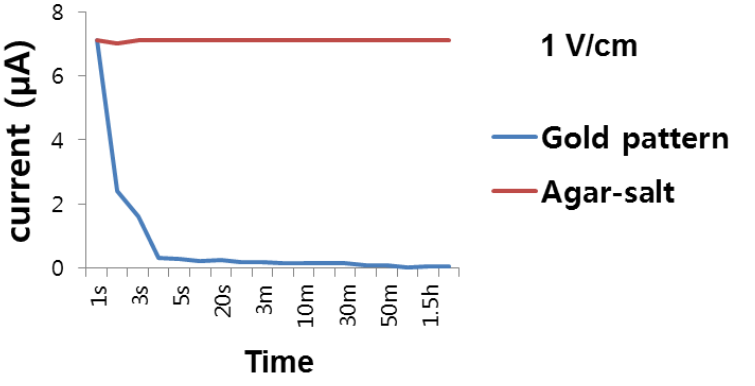

Figure. 17. Current pattern of gold pattern system and agar salt bridge system. The current is stable in gar salt bridge system.

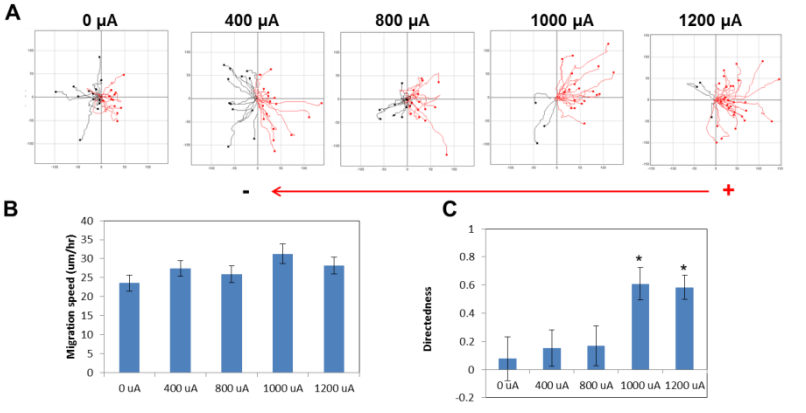

Figure. 18. Migration assay of hMSCs by electrotaxis. (A) Cell tracking data, (B) migration speed and (C) directedness of hMSCs in various electric current condition (0, 400, 800, 1000, 1200 μA).

E. Migration of hMSCs into PCL scaffold by electrotaxis

Before we fabricate the scaffold, intensity of current in the scaffold should be distributed homogeneously first. So we simulated the current distribution in scaffold using comsol physics computer program. We designed lattice structure for difficult infiltration without any stimulation. The color represented the current intensity and current flowed along the space next to the acrossed area, so current observed that homogeneously distributed (Fig. 19). 3D prined PCL scaffold was fabricated and SEM image showed that the lattice structure was well formed (Fig. 20).

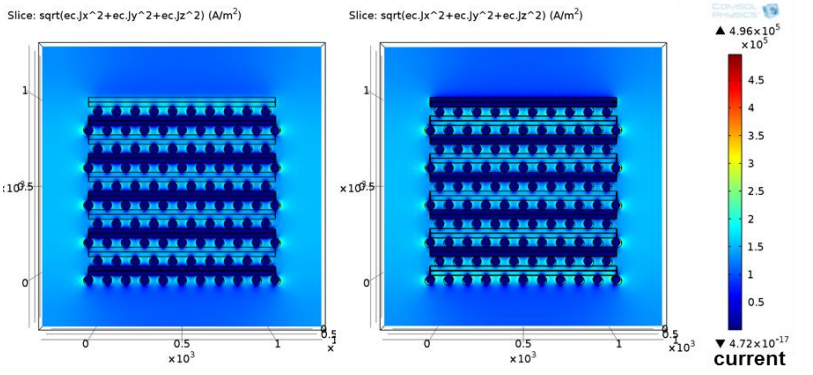

Figure. 19. The simulation of current distribution in PCL scaffold. The electric stimulation was applied homogeneously into the PCL scaffold.

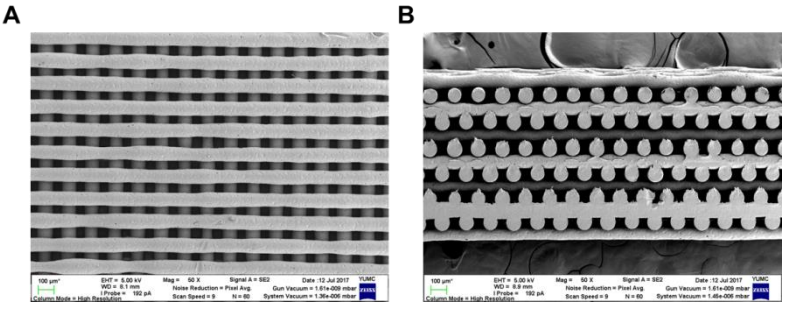

Figure. 20. SEM images of 3d printed PCL scaffold. (A) Surface and (B) cross-sectional SEM image of PCL scaffold.

With this scaffold, we identify the infiltration test. First we need to find the appropriate stimulation condition. Cell seeded into scaffold incubation 1day then 1000uA electric treated for 3h. Each day we treated same electric stimulation and compared (Fig. 21A). As a result, if there was no electric treatment, cell stayed near the surface of scaffold. However electric stimulation enhanced the infiltration of cells. More infiltration showed when electric treatment 2 times than 1time. Between 3times and 2times looks similar infiltration. For our 1mm thick scaffold, electric treatment 2 times is enough to enhancing the infiltration of cells (Fig. 21B).

To identify the infiltration and distribution of cells into the scaffold, we treated 2 times of electric stimulation then observed using confocal microscope. As we seen, if there was no electric stimulation, hmscs almost stayed near the surface until 28 days However, electric treatment was applied, the cell infiltration enhanced and cells distributed homogeneously until 28 days (Fig. 22A). We also identified the stemness of hmsc and at day 28 the stemcell marker cd-105 was observed so this electric stimulation was stable condition to enhance the infiltration into stem cell (Fig. 22B).

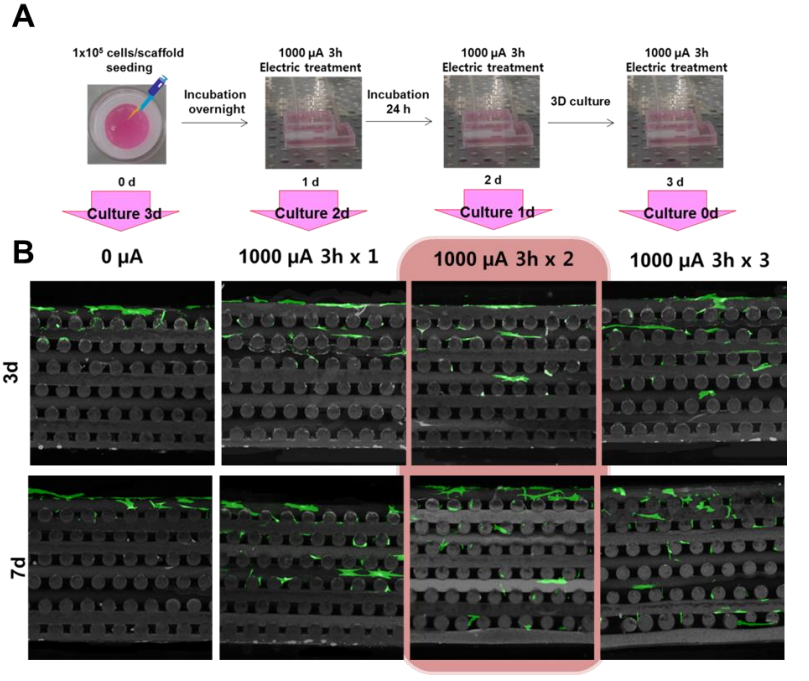

Figure. 21. hMSC migration into PCL scaffold by electric stimulation condition. (A) The schematic of electrotaxis in 3-D PCL scaffold. (B) Comparison of hMSC migration into PCL scaffold at 3 d and 7d by number of electric treatments.

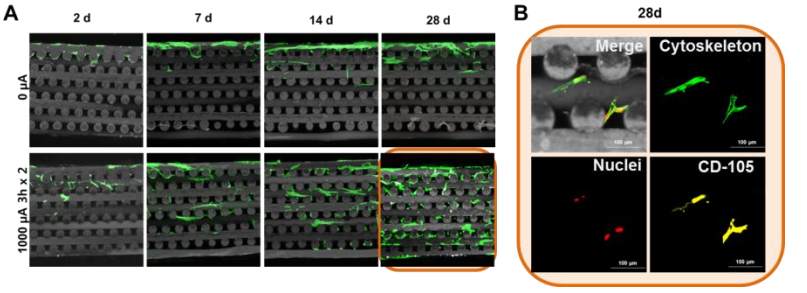

Figure. 22. Homogeneous distribution of hMSCs in PCL scaffold by electric stimulation. (A) hMSC distribution in PCL scaffold under 0 or 1000 μA treatment condition at 2, 7, 14, 28 d. (B) Immunofluorescence images of hMSC under 1000 μA treatment condition at 28d. The nuclei were stained with PI, the actin cytoskeleton was stained with Alexa (488)-conjugated phalloidin (green), and CD-105 were stained with Texas Red (red). Scale bar = 100 μm.

F. Histological evaluation of implanted PCL scaffold

The PCL scaffold implantation group (control) at 1 week (Fig. 23A) showed a typical morphology of porous PCL scaffold (void space) with very few nuclei. The hMSC seeded PCL scaffold implantation group (hO-EX) at 1 week (Fig. 23B) showed an accumulation of cells around upper surface of PCL scaffold where the hMSCs seeded before implantation and few nuclei were observed inside the scaffold. The both of hMSC seeding and electric stimulation treated PCL scaffold implantation group (hO-EO) at 1 week (Fig. 23C) showed that many cells were stained in the middle of scaffold. In 2 weeks of control group (Fig. 23D), there were no signs of vascular areas however dark red stained areas (white arrows) were observed in hO-EX and hO-EO (Fig. 23E, F). Especially the vascular area was observed in the middle of PCL scaffold in hO-EO group. At 3 weeks, vascular area of control and hO-EX group were observed near the edge of scaffold and middle of scaffold (Fig. 23G, H) however vascular area was observed in the middle of scaffold of hO-EX group (Fig. 23I). Also the pink stained thread-like network became denser and darker suggesting the presence of collagen fibers.

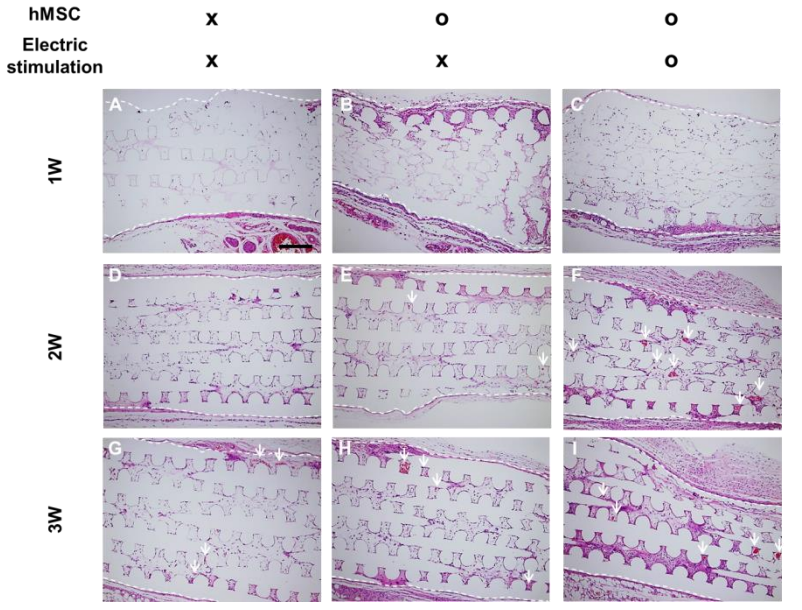

Figure. 23. Representative Hematoxylin and Eosin (H&E) images after 1, 2 and 3 weeks of implantation. After 1 week implantation of (A) PCL scaffold (B) hMSC seeded PCL scaffold (C) hMSC seeded PCL scaffold under 1000 μA treatment condition. After 2 weeks implantation of (D) PCL scaffold (E) hMSC seeded PCL scaffold (F) hMSC seeded PCL scaffold under 1000 μA treatment condition. After 3 weeks implantation of (G) PCL scaffold (H) hMSC seeded PCL scaffold (I) hMSC seeded PCL scaffold under 1000 μA treatment condition. The arrows indicate the circular and ellipsoid cross section of the vascular structures. The dashed line represents the outer edge of scaffold. Scale bar = 200 μm.

4. Discussion

In our previous study, the optimal condition of nHDFs directional migration by the electrotaxis was identified and the Golgi polarization was observed during the electrotaxis.[17] To identify the effect of electrotaxis on the nHDF migration when the Golgi polarization was blocked, 1 μM of BFA was treated before the dc EF treatment to the cells. Brefeldin A (BFA) prevents the assembly of cytosolic coat proteins onto Golgi membranes, resulting in the formation of Golgi tubules and prevents tubule detachment from the Golgi structure which then fuses with the endoplasmic reticulum (ER). This leads to rapid diffusion of Golgi membrane into the ER and disruption of Golgi. BFA at high concentrations of 2-5 mg/ml (~18 mM) causes this rapid dispersal of the Golgi within 5-8 min after addition of the.[19-21] We used a concentration of BFA (5 mM) and found the same quick dispersal of the Golgi apparatus. This treatment resulted in discoid cell morphology. It is impossible to analyze Golgi polarization and cell migration as there is no visible Golgi staining and the cells do not move. So, 1 μM of BFA was chosen for this experiment.

The Golgi polarization of each condition assumed similar aspect

with the directedness results. There is no significant difference that the Golgi polarization of 0 V/cm for 4 h between 45^{o} and 315^{o} or between 135^{o} and 225^{o}. Golgi polarization between 45^{o} and 315^{o} means right, 135^{o} and 225^{o} indicates left. In 1 V/cm, the Golgi polarization was increased toward right for first 2 h, then significantly increased toward left for rest 2 h. However, in 1 V/cm þ BFA at 2 h maintained the high percent of Golgi polarization toward right for 4 hours even though the direction of dc EF was reversed. These results indicated that Golgi polarization is more important to the directional migration of the nHDFs than the dc EF. Also, the induction of Golgi polarization is necessary to induce the directional migration using the dc EF.

Golgi polarization is an important feature of cell polarization. This is critically involved in directional cell migration, as the Golgi apparatus plays an important role in anterograde supply of membrane components to the leading edge for membrane protrusion. PI 3-kinase and Src are required for Golgi polarization in the directional cell migration of fibroblast cells. The two kinases are activated at the leading edge of fibroblasts responding to platelet-derived growth factor gradients and keratinocytes in the scratch-wound model. Rho family members of small GTPases, mainly Rho, Rac1 and cdc42, are important for cell polarity establishment. In response to scratch wounds, astrocytes and fibroblasts polarize the Golgi into the wound, which requires cdc42. Polarization of endothelial cells in response to shear stress, however, is not mediated by cdc42 or PI 3-kinases, but by Rho and Rac. This suggests that EF-induced Golgi polarization may involve some different signalling pathways partially bypassing Rho small GTPases or PI 3-kinases. The exact mechanism of directional migration by physical stimulation is unclear, however the golgi polarization data suggest that cell sensed the physical stimulation and showed directional migration, not by the push force of fluid shear stress or electrical forces of electrotaxis.

Hydrophilicity and hydrophobicity is related with the attachment of cells rather than the direction of migration. Previous studies about electrotaxis were performed with cells on the non-conductive surfaces, so non-conductive material was selected to fabricate the 3-D scaffold. Electrotaxis study of non-conductive surface is different from conductive surface, because the electric current flows on the surface of conductive scaffold too. Breast cancer cell; MDA-MB-231 was migrated to anode under 1 V/cm EF which was seeded on the indium-tin oxide coated glass.[22] The growth of NIH-3T3 fibroblast on the Pani-based scaffold was increased by electric stimulation,[23] and viability, mitochondrial activity, IL-6 and IL-8 secretion of human cutaneous fibroblasts on the PPy–PLLA films were enhanced by electric stimulation.[24,25] However, it is also worth noting that applying an electrical current through the conductive polymer will gradually increase its resistivity, thereby limiting its useful life time,[26] and that long-term exposure of cells to high electrical currents (in the range of 1 mA and above) can have a cytotoxic effect.[27] For these reason, the non-conductive scaffold was studied for the effect of electrotaxis on the cell migration into 3-d scaffold.

5. Conclusion

In closing, we identified Physical stimulations (electric current) could control the directional migration of cells. The study about Golgi and electrotaxis indicated that Golgi polarization is more important to the directional migration of the nHDFs than the dc EF. The migration of hMSCs into scaffold was enhanced by the control of migration using physical stimulations. Also, in-vitro and in-vivo, the directional migration by electrotaxis enhanced the homogeneous distribution of cells in 3-D PCL scaffold.

References

1. Levin M. Morphogenetic fields in embryogenesis, regeneration, and cancer: non-local control of complex

patterning. Biosystems 2012; 109: 243–261

2. McCaig CD. Electric fields, contact guidance and the direction of nerve growth. J Embryol Exp Morphol 1986;94: 245–255.

3. McCaig CD, Song B, Rajnicek AM. Electrical dimensions in cell science. J Cell Sci 2009;122: 4267–4276.

4. Metcalf M, Borgens RB. Weak applied voltages interfere with amphibian morphogenesis and pattern. J Exp Zool 1994;268:323–338.

5. Messerli MA, Graham DM. Extracellular electrical fields direct wound healing and regeneration. Biol Bull 2011;221: 79–92.

6. Robinson KR, Messerli MA. Left/right, up/down: the role of endogenous electrical fields as directional signals in development, repair and invasion. Bioessays 2003;25: 759–766.

7. Zhao Z, Qin L, Reid B, Pu J, Hara T, Zhao M. Directing migration of endothelial progenitor cells with applied DC electric fields. Stem Cell Res 2012;8:38-48.

8. Zhao Z, Watt C, Karystinou A, Roelofs AJ, Caig MC, Gibson IR. Directed migration of human bone marrow mesenchymal stem cells in a physiological direct current electric field. Eur Cell Mater 2011;22:344-58.

9. Guo A, Song B, Reid B, Gu1 Y, Forrester JV, Jahoda CAV, et al. Effects of physiological electric fields on migration of human dermal fibroblasts. J Invest Dermatol 2010;130:2320-7.

10. Jaffe LF, Vanable JW. Electric fields and wound healing. Clin Dermatol 1984;2:34-44.

11. McCaig CD, Zhao M. Physiological electrical fields modify cell behaviour. Bioessays 1997;19:819-26.

12. McCaig CD, Rajnicek AM, Song B, Zhao M, Has electrical growth cone guidance found its potential. Trends Neurosci 2002;25:354-9.

13. Nuccitelli R. A role for endogenous electric fields in wound healing. Curr Top Dev Biol 2003;58:1-26.

14. Nuccitelli R. Endogenous electric fields in embryos during development, regeneration and wound healing. Radiat Prot

Dosim 2003;106:375-83.

15. Ojingwa JC, Isseroff RR. Electrical stimulation of wound healing. J Invest Dermatol 2003;121:1-12.

16. Robinson KR, Messerli MA, Left/right, up/down: the role of endogenous electrical fields as directional signals in development, repair and invasion. Bioessays 2003;25:759-66.

17. Kim MS, Lee MH, Kwon, BJ, Park JC. Control of neonatal human dermal fibroblast migration on poly (lactic-co-glycolic acid)-coated surfaces by electrotaxis. J Tissue Eng Regen Med 2017;11:862-8

18. Ma Z, Gao C, Gong Y. Cartilage tissue engineering PLLA scaffold with surface immobilized collagen and basic fibroblast growth factor. Biomaterials 2005; 26:1253-9.

19. Presley JF, Smith C, Hirschberg K, Miller C, Cole NB, Zaal KJ, Lippincott-Schwartz J. Golgi membrane dynamics. Mol Biol Cell 1998;9:1617-26.

20. Sciaky N, Presley J, Smith C, Zaal KJM, Cole N, Moreira JE, et al. Lippincott-Schwartz, Golgi tubule traffic and the

effects of brefeldin A visualized in living cells. J Cell Biol 1997;139:1137-55.

21. Hirschberg k, Miller CM, Ellenberg J, Presley JF, Siggia ED, Phair RD, el al. Kinetic analysis of secretory protein traffic and characterization of Golgi to plasma membrane transport intermediates in living cells. J Cell Biol 1998;143-1485-503.

22. Kim MS, Lee MH, Kwon BJ, Seo HJ, Koo MA, You KE, Kim D, Park JC. Effects of direct current electric-field using ITO plate on breast cancer cell migration. Biomaterials Research 2014:18:10-15.

23. Jeong SI, Jun ID, Choi MJ, Nho YC, Lee YM, Shin H. Development of electroactive and elastic nanofibers that contain polyaniline and poly(Llactide-co-e-caprolactone) for the control of cell adhesion. Macromol Biosci 2008;8:627-37.

24. Shi G, Rouabhia M, Meng S, Zhang Z. Electrical stimulation enhances viability of human cutaneous fibroblasts on conductive biodegradable substrates. J Biomed Mater Res 2008;84:1026-37.

25. Shi G, Zhang Z, Rouabhia M. The regulation of cell functions electrically using biodegradable polypyrrole–polylactide conductors. Biomaterials 2008;29:3792-8.

26. Zhang Z. Electrically conductive biodegradable polymer composite for nerve regeneration: electricity-stimulated neurite outgrowth and axon regeneration. Artif Organs 2007;31:13-22.

27. Richardson RT. The effect of polypyrrole with incorporated neurotrophin-3 on the promotion of neurite outgrowth from auditory neurons. Biomaterials 2007;28:513-23.

IV. Evaluation of cell homogeneity by migration analysis

1. Introduction

In recent years there have been tremendous studies in the stem cell therapy, because it has some advantages which can restore function to damaged or diseased tissue, avoid host rejection and reduce inflammation throughout the body without the use of immunosuppressive drugs.[1] Specifically adult stem cells, multipotent cells with the capacity to promote angiogenesis, differentiate to produce multiple types of connective tissue and down-regulate an inflammatory response are the focus of a multitude of clinical studies currently under way. The stem cells are being explored to regenerate damaged tissue and treat inflammation, resulting from cardiovascular disease and myocardial infarction, brain and spinal cord injury, stroke, diabetes, cartilage and bone injury.[2] In stem cell therapy, the differentiated cell ratio is very important because there is a risk to form a tumour when the undifferentiated cells were implanted into body.[3] However the current differentiation protocols of human stem cells are not able to synchronize the birth and development of cell populations to the extent seen in normal development, and consequently cells at different stages of maturation are present in

such cultures, causing a cellular heterogeneity that impedes experimental and clinical utility.[4-7] To solve these problems, the homogeneity of stem cells needed to be identified before the application and the evaluation technique of stem cell homogeneity is strongly demanded. Flow cytometric analysis and fluorescence-activated cell sorting (FACS) provide separation of cellular populations based on fluorescent labeling, for example according to surface antigens.[8,9] After such work has been accomplished, defined combinations of surface markers can be used to identify and to isolate specific stem cell markers by FACS or by immunomagnetic cell separation (MACS).[10] Such stem cell selection procedures and marker sets will enable the analysis, characterization, and separation of distinct subpopulations of stem cells for basic studies of stem cell biology, development, and potential therapeutic application. However these evaluation techniques of stem cells took a time and needed many preparations, so new stem cell selection methods are needed to realize the possible scientific and clinical benefits of using human stem cells. The cell migration is influenced by the direct electric current and this phenomenon is called ‘Electrotaxis’.[11] The direction or migration speed of cells was influenced by the direct current and the electrotaxis was specific to the cell types. Because of this

specificity, electrotaxis is very helpful to study the cell migration characteristics and also this electrotaxis could be a characteristic of each cell. Here we suggest an electrotaxis analysis as a new method to evaluate the homogeneity of stem cells.

2. Materials and Methods

A. Cell Culture and Osteogenic differentiation

Adipose derived stem cell (ADSC, Lonza, Switzerland) were cultured in adipose derived stem cell growth medium (ADSCGM, Lonza). Human mesenchymal stem cells (hMSC, Lonza, Basel, Switzerland) were cultured in mesenchymal stem cell growth medium (MSCGM, Lonza). Tonsil mesenchymal stem cells (TMSC) were provided by Dr. Jo in Ewha woman's university (Seoul, Korea) and cultured in DMEM (Welgene, Seoul, Korea).[12] Cells were incubated at 37 ℃ in a 5% CO_2 atmosphere. ADSC, hMSC and TMSC passages between 3 and 5 were used in all experiments. Osteogenic differentiation (OsD) of stem cells was performed at defined passages 3-5. To promote osteogenic differentiation, cells were seeded at a density of 3.1×10^3 cells/cm^2 into 75 T flask and cultured in ADSCGM for ADSC, MSCGM for hMSC and DMEM for TMSC until they reached 80% confluence. As soon as subconfluence was reached, osteogenic differentiation of cells was induced by feeding them for 2 weeks, twice a week with osteogenic induction medium for ADSC and hMSC. DMEM with 50 μg/ml ascorbic acid, 10 mM B-glycerophosphate, 10 nM dexamethasone was used for TMSC osteogenic differentiation.[12]

B. Preperation of stem cell vs. OsD cell mixture

The stem cells were cultured in osteogenic induction medium to make the OsD cells. The stem cells and OsD cells were mixed at ratio 3:7, 5:5, 7:3. OsD 3, 7, 14d cells means that the cells which were culture in osteogenic induction medium for 3, 7, 14 days. To make 3:7 ratio of mixture, for example stem cells and OsD cells were detached by trypsin and 3×10^3 stem cells, 7×10^3 OsD cells were injected to 1 ml of suspension.

C. Electrotaxis on stem cells

To apply a direct electric current to stem cells and osteogenic differentiated cells, we used a customized agar-salt electrotaxis incubator and chamber system.[13,14] The electrotaxis chamber and incubator system consisted of the incubator system and electrotaxis chamber. The incubator system was installed with a microscope to observe live cells and the electrotaxis chamber applies a direct electric current to the cells. The incubator which maintains the proper growth environment (CO_2 5%, 37 ℃) is regulated by a temperature and gas composition-controlling program (CCP ver. 3.8, Live Cell Instrument, Seoul, Korea). A cell seeded slide glass was mounted on the chamber bottom, and the chamber top and silicon gasket were placed on top of the slide. At the end of the chamber top was connected with 2% agar-salt bridge. To sterilize the chamber, the chamber was dipped in 70% ethanol and washed three times with distilled water (DW). The cells were seeded at 3×10^3 cells density on the slide glass with silicon O-ring (inner diameter 16 mm) and incubated for 16~24 h in the CO_2 incubator.

D. Immunofluorescence Observation

Stem cells and osteogenic differentiation were observed by immunofluorescence staining. Stem cells and osteogenic differentiated cells were fixed with 4% formaldehyde for 30 min at room temperature and then washed 3 times with PBS. Cells were permeabilized with 0.1% Triton X-100 in PBS for 5 min at room temperature and rinsed 3 times with PBS. 3% bovine serum albumin was treated for 30 min at room temperature and cells were incubated with a RUNX2 primary antibody (dilution 1:100, BD Transduction Laboratories TM, BD Biosciences, CA, USA) overnight at 4 ℃. Cells were then washed at least 3 times with PBS and treated with CD-105 primary antibody (dilution 1:100, BD Transduction Laboratories TM) for 1 h. After 3 times washing with PBS, Alexa (488) (5 U/ml, Invitrogen, Carlsbad, CA, USA) for the RUNX2 and goat anti-mouse IgG conjugated with Texas Red (dilution 1:50, Santa Cruz, CA, USA) for CD105, treated for 1 h at room temperature in the dark. After PBS washing, cells were treated with Hoechst #33258 (Sigma, St. Louis, MO, USA) for 5 min at room temperature in the dark. The cell seeded slide glass was then mounted on the fluorescence-inverted microscope (LSM700, Carl Zeiss, New York, USA) and observed.

E. Homogeneity evaluation of stem cells by electrotaxis analysis

To evaluate the stem cell homogeneity, we used migration speed histograms and electrotaxis analysis. The cell migration data were analyzed using SAS software (version 9.4, SAS Inc., Cary, NC, USA). The threshold of stem cell migration speed vs. osteogenic differentiated cells at day 3, 7, 14 was determined by optimal cut-off value (Youden's J index).[15] This index can be defined as J = max {sensitivity of all possible threshold values (Se(c)) + specificity of all possible threshold values (Sp(c)) − 1} and ranges between 0 and 1. Complete separation of the distributions of the marker values for the diseased and healthy populations results in J = 1 whereas complete overlap gives J = 0.[15] J provides a criterion for choosing the "optimal" threshold value (c*), the threshold value for which Se(c) + Sp(c) − 1 is maximized.[16]

F. Statistical Analysis.

Data were reported as means ± standard error of the mean (SEM). Means were compared using one-way analyses of Student's t-tests. A value of $p < 0.05$ is considered statistically significant.

3. Results

A. Osteogenic differentiation of stem cells

Mesenchymal stem cells (MSC) are identified as a multipotent cell population in the adult organism able to be induced to express adipogenic, osteogenic and chondrogenic markers.[17–21] Osteogenic differentiation was confirmed by the detection of stem cell marker (CD-105) and osteogenic differentiation marker (RUNX2) by immunofluorescence staining. (Fig. 24.) CD-105 was strongly detected at OsD day 0 and day 3 but RUNX2 was not expressed at the same period. RUNX2 was detected at day 7 while the intensity of CD-105 decreased at OsD day 7. At day 14 of OsD, the intensity of RUNX2 was increased but CD-105 was not detected. These results suggested that ADSC, hMSC and TMSC were fully differentiated at day 14 by using the osteogenic differentiation media. The effect of electric current on the osteogenic differentiation was also identified. S1 showed that CD-105 of ADSC which were treated by 1000 μA of electric current was detected at 7, 14, 21 days after electric treatment, however RUNX2 was not observed. In hMSC and TMSC case, CD-105 and RUNX2 showed same results as ADSC.

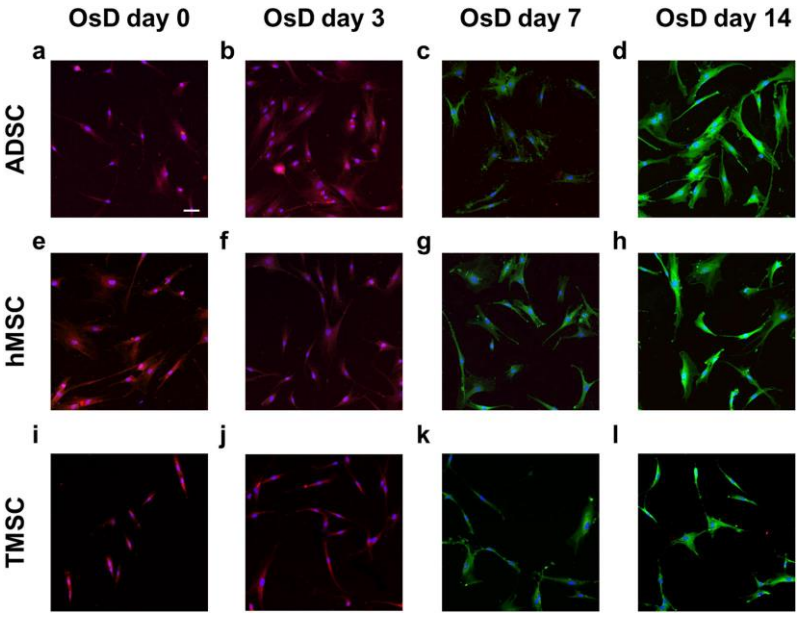

Figure. 24. The immunofluorescence images of stem cells and osteogenic differentiated stem cells. The immunofluorescence images of ADSC osteogenic differentiation at (A) day 0, (B) day 3, (C) day 7, (D) day 14. The immunofluorescence images of hMSC osteogenic differentiation at (E) day 0, (F) day 3, (G) day 7, (H) day 14. The immunofluorescence images of TMSC osteogenic differentiation at (I) day 0, (J) day 3, (K) day 7, (L) day 14. The nuclei were stained with Hoechst #33258 (blue), the RUNX2 (osteogenic differentiation marker) was stained with Alexa (488) (green), and CD-105 (ADSC marker) was stained with Texas Red conjugated antibody (red). Scale bar = 100 μm.

B. Electric current induced directional migration of stem cells and osteogenic differentiated cells

To analyse the change of migration pattern of stem cells and osteogenic differentiated cells, we used electrotaxis. Figure 25 showed the cell tracking data of ADSC, hMSC, TMSC and osteogenic differentiated cells at OsD day 3, 7, 14 with 0, 1000 μA for 3 h. ADSC, hMSC and TMSC showed no directional migration with no electric current, however moved to the anode when the 1000 μA of electric current was applied to the cells. The migration speed was significantly decreased at OsD day 7 and 14 compared to the day 0 (Fig. 25A,C,E). The migration speed was not affected by the electric current. However, x directedness of electric current treated group was significantly increased compared to day 0 with 0 μA (Fig. 25B,D,F). These results indicated that the more MSCs osteogenic differentiated, the more migration speed decreased but the direction of MSC migration by electrotaxis was not affected. Therefore we could use the migration speed as an independent factor of electrotaxis analysis.

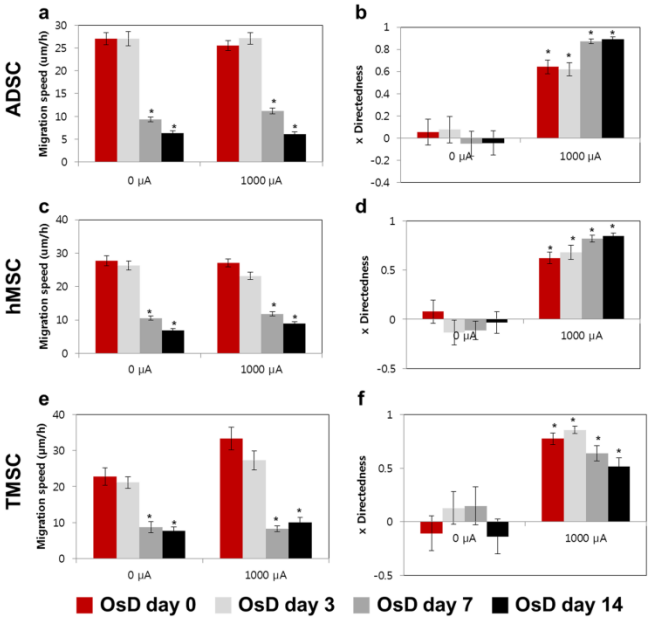

Figure. 25. Migration data of stem cells and osteogenic differentiated cells. (A) Migration speed of ADSC and osteogenic differentiated cells, (B) x directedness of ADSC and osteogenic differentiated cells at day 0, 3, 7, 14 with 0, 1000 μA for 3 h. (C) Migration speed of hMSC and osteogenic differentiated cells, (D) x directedness of hMSC and osteogenic differentiated cells at day 0, 3, 7, 14 with 0, 1000 μA for 3 h. (E) Migration speed of TMSC and osteogenic differentiated cells, (F) x directedness of TMSC and osteogenic differentiated cells at day 0, 3, 7, 14 with 0, 1000 μA for 3 h. *$p < 0.05$ compared to the 0 d with 0 μA for 3 h.

C. Appropriate current condition for migration analysis

To evaluate the effect of electrotaxis on the stem cell viability, Live/Dead assay and MTT assay were performed. The Live/Dead assay was carried out right after the 1000 μA of electric current. Only green dyed cells which mean the live cells were observed in ADSC, hMSC and TMSC case, and there were no dead cells (Fig. 26A~F). In MTT assay data at 1d and 3d, there were no differences between 0 μA and 1000 μA of electric treatment on stem cells (Fig. 26G~I). These results showed that stem cell viability was not affected by 1000 μA of electric current.

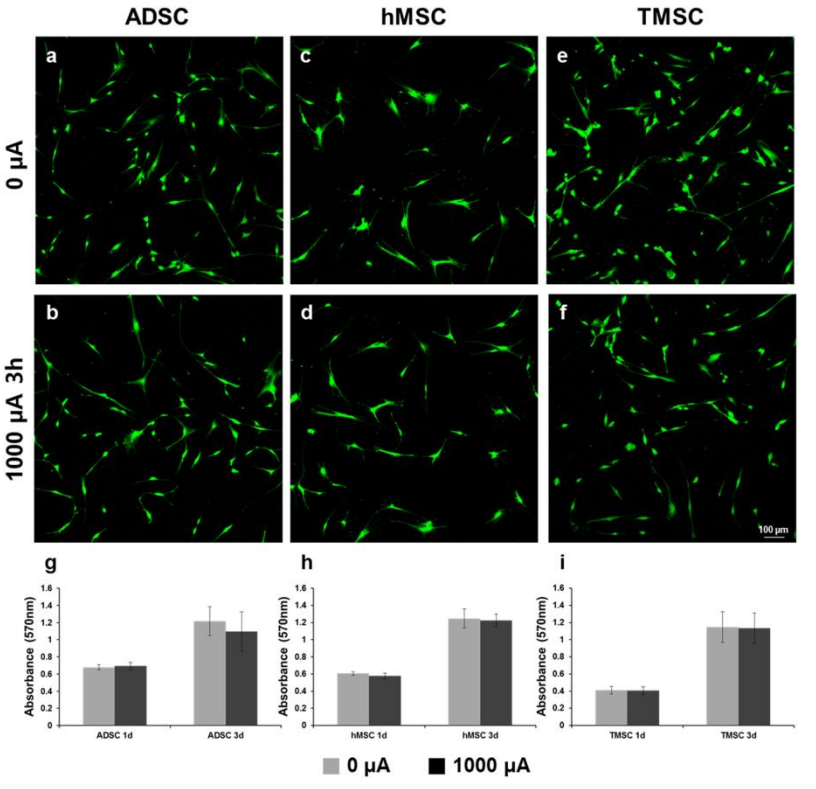

Figure. 26. The effect of direct electric current on the cell viability. The LIVE/DEAD assay images of (A) ADSC under 0 μA, (B) ADSC under 1000 μA for 3 h, (C) hMSC under 0 μA, (D) hMSC under 1000 μA for 3 h, (E) TMSC under 0 μA, (F) TMSC under 1000 μA for 3 h (live cells: green, Calcein AM/dead cells: red, EthD-1). Scale bar = 100 μm. The MTT assay of (G) ADSC, (H) hMSC, (I) TMSC for 1, 3d culture after 0 or 1000 μA treatment for 3 h.

D. Evaluation of cell homogeneity by electrotaxis analysis

To evaluate the homogeneity of stem cells, the mixtures of stem cells and osteogenic differentiated cells was prepared; ADSC vs. osteogenic differentiated cell, hMSC vs. osteogenic differentiated cell, TMSC vs. osteogenic differentiated cell. Each mixture group has 3 different ratios and the ratios were 7:3, 5:5, 3:7. We identify the homogeneity of stem cells using the stem cell marker and osteogenic differentiation maker, then these homogeneity data by markers were compared with homogeneity data by electrotaxis analysis. Figure 27A~I showed the fluorescence images of ADSC and osteogenic differentiated cell population at OsD day 3, 7, 14. The population of ADSC could be identified at OsD day 7 and day 14 by OsD marker and stem cell marker (Fig. 27D~I). Before evaluate the ADSC homogeneity by electrotaxis analysis, the migration speed histogram of ADSC and osteogenic differentiated cell mixture was performed first. The frequency of ADSC and ratio 3:7, 5:5, 7:3 was almost matched at OsD day 3 (Fig. 27J). However, the frequency of ADSC and ratio 3:7, 5:5, 7:3 has a difference at OsD day 7, day 14 (Fig. 27K,L). These results mean that the heterogeneity of mixture at 3d could not be detected by fluorescence images or electrotaxis analysis, however the

population of ADSC and osteogenic differentiated cells was possible to be detected by RUNX2 and CD-105 marker, and electrotaxis analysis at day 7, day 14 (Fig. 27D~L). The same analysis was applied to hMSC and TMSC mixture, too. The population of hMSC could be identified at OsD day 7 and day 14 by OsD marker and stem cell marker, but not be identified at OsD day 3 (Fig. 28A~I). The migration speed histogram of hMSC and osteogenic differentiated cell mixture showed that the frequency of hMSC and ratio 3:7, 5:5, 7:3 was almost matched at OsD 3d (Fig. 28J). However, the frequency of hMSC and ratio 3:7, 5:5, 7:3 has a difference at OsD day 7, day 14 (Fig. 28K,L). In TMSC and OsD mixture, similar data were also obtained (Fig. 29). Finally we evaluate the homogeneity of MSCs by electrotaxis and Youden index analysis (Fig. 30). In mixture of ADSC and OsD day 3 cells, the percentage of ADSC was 91.7 ± 4.4% at 3:7 ratio, 85.0 ± 5.8% at 5:5 ratio, 81.7 ± 7.3% at 7:3 ratio. In mixture of ADSC and OsD day 7 cells, the percentage of ADSC was 30.0 ± 2.9% at 3:7 ratio, 45.0 ± 2.9% at 5:5 ratio, 70.0 ± 5.0% at 7:3 ratio. In mixture of ADSC and OsD day 14 cells, the percentage of ADSC was 35.0 ± 2.9% at 3:7 ratio, 45.0 ± 5.8% at 5:5 ratio, 65.0 ± 2.9% at 7:3 ratio (Fig. 30A). In mixture of hMSC and OsD day 3 cells, the percentage of hMSC was 80.0 ± 2.9% at 3:7 ratio, 95.0 ± 5.0% at

5:5 ratio, 81.7 ± 9.3% at 7:3 ratio. In mixture of hMSC and OsD day 7 cells, the percentage of hMSC was 30.0 ± 5.0% at 3:7 ratio, 50.0 ± 2.9% at 5:5 ratio, 65.0 ± 5.8% at 7:3 ratio. In mixture of hMSC and OsD day 14 cells, the percentage of hMSC was 35.0 ± 7.6% at 66.0 ± 2.0% at 7:3 ratio (Fig. 30B). In mixture of TMSC and OsD day 14 cells, the percentage of TMSC was 30.0 ± 58% at 3:7 ratio, 53.3 ± 4.4% at 5:5 ratio, 73.3 ± 1.7% at 7:3 ratio (Fig. 30C). The percentage of MSCs in mixture with OsD cells was almost matched with each ratio, so these results suggested that the possibility about the evaluation of MSCs homogeneity by electrotaxis analysis was identified.

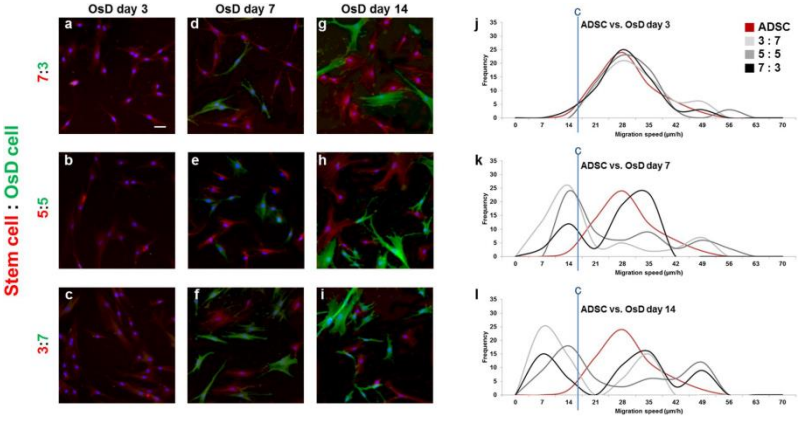

Figure. 27. Mixture of ADSC and osteogenic differentiated cells at different OsD days. The immunofluorescence images of ADSC and osteogenic differentiated cells mixture ratio of (A) 7:3, (B) 5:5, (C) 3:7 at day 3, (D) 7:3, (E) 5:5, (F) 3:7 at day 7, and (G) 7:3, (H) 5:5, (I) 3:7 at day 14. The histogram of ADSC and osteogenic differentiated cell mixture using electrotaxis analysis and Youden index under 1000 μA at (J) day 3, (K) day 7, (L) day 14. Cut point of ADSC vs. osteogenic differentiated cells was 18.71 μm/h. Scale bar = 100 μm.

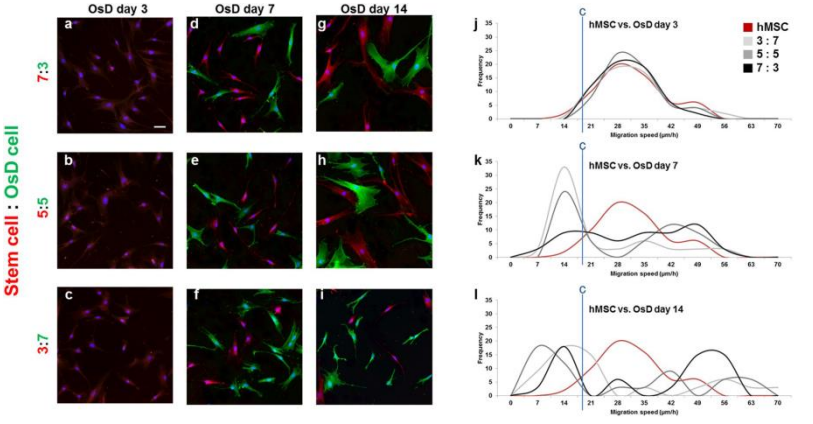

Figure. 28. Mixture of hMSC and osteogenic differentiated cells at different OsD days. The immunofluorescence images of hMSC and osteogenic differentiated cells mixture ratio of (A) 7:3, (B) 5:5, (C) 3:7 at day 3, (D) 7:3, (E) 5:5, (F) 3:7 at day 7, and (G) 7:3, (H) 5:5, (I) 3:7 at day 14. The histogram of hMSC and osteogenic differentiated cell mixture using electrotaxis analysis and Youden index under 1000 μA at (J) day 3, (K) day 7, (L) day 14. Cut point of hMSC vs. osteogenic differentiated cells was 18.73 μm/h. Scale bar = 100 μm.

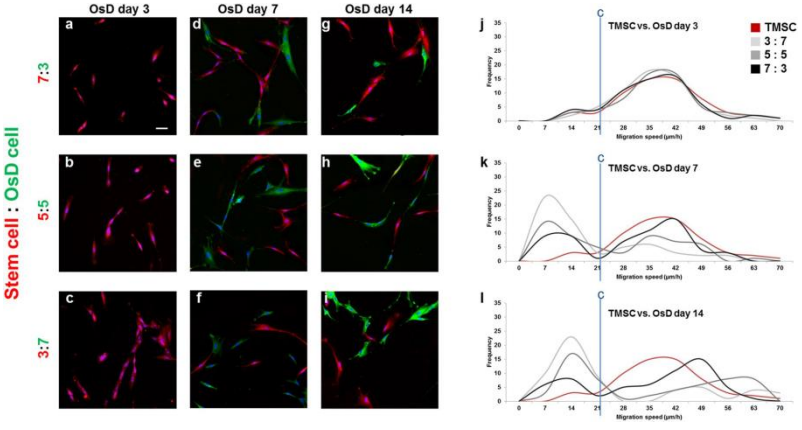

Figure. 29. Mixture of TMSC and osteogenic differentiated cells at different OsD days. The immunofluorescence images of TMSC and osteogenic differentiated cells mixture ratio of (A) 7:3, (B) 5:5, (C) 3:7 at day 3, (D) 7:3, (E) 5:5, (F) 3:7 at day 7, and (G) 7:3, (H) 5:5, (I) 3:7 at day 14. The histogram of TMSC and osteogenic differentiated cell mixture using electrotaxis analysis and Youden index under 1000 μA at (J) day 3, (K) day 7, (L) day 14. Cut point of TMSC vs. osteogenic differentiated cells was 22.42 μm/h. Scale bar = 100 μm.

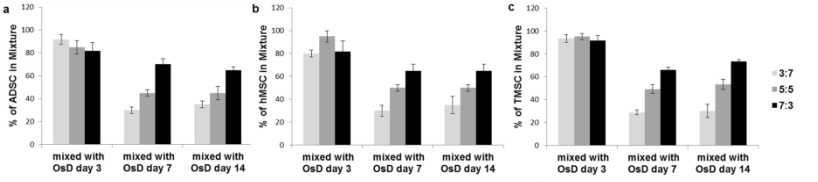

Figure. 30. Homogeneity evaluation of mesenchymal stem cells based on electrotaxis analysis. (A) Evaluation data of ADSC homogeneity in mixture of ADSC and osteogenic differentiated cells. (B) Evaluation data of hMSC homogeneity in mixture of hMSC and osteogenic differentiated cells. (C) Evaluation data of TMSC homogeneity in mixture of TMSC and osteogenic differentiated cells.

4. Discussion

The heterogeneity of stem cell therapy products hampers not only the fast translation of research into clinics but also the proper interpretation of clinical trial data. This heterogeneity could originate from intrinsically heterogeneous initial cell populations and additional diversity of cell populations during the stem cell culture process.[7] Thus, as important as it is to implement a standardized stem cell culture process, evaluation technique of stem cell homogeneity to reduce the heterogeneity is critical to stem cell therapy. There are some studies that hypoxic environment promoted the osteogenic differentiation of stem cells.[22, 23] Other reports demonstrated that human bone marrow-derived MSCs cultured under hypoxia showed a diminished capacity to differentiate into adipocytes and osteocytes, supporting the notion that low oxygen tension promotes an undifferentiated state.[24-26] Especially the current differentiation protocols lead to unsynchronized the birth and development of cell populations and different differentiation stages.[4–7] According to these studies, stem cell quality control is very important when we culture the stem cells in stem cell differentiation.

Direct current electric fields are present naturally at wounds in a

variety of different tissues and are a powerful directional guidance cue for epithelial cells, fibroblasts, vascular endothelial cells, keratinocytes, endothelial progenitor cells, and neurons. Directed migration of cells in a DC EF is highly cell-type specific, since some cell types migrate cathodically and others anodically.[27] Here, 3 types of MSCs showed strong anodal electrotaxis in physiological electric current (Fig. 25). However, mouse adipose-derived stromal cells (mASC) migrated towards the cathode in response to EFs.[28] In our hands, osteogenic differentiated cells from ADSC, hMSC and TMSC migrated anodally (Fig. 25). This difference in electrotaxis could be related to differences in cell types, tissue sources and species, thereby emphasising the need for comprehensive studies of the effects of EF application on a case-by-case basis. The underlying mechanisms of MSC electrotaxis for each cell type need to be clarified, nevertheless it is believed that the electrotaxis is the specificity of each cells. The direct current induced directional migration of hMSC but did not effect on osteogenic differentiation,[26] so our electrotaxis analysis technique which enables the real time observation of cell characteristics during cell cultures is a candidate for stem cell quality control method.

For some stem cell types, the initial cell populations can be isolated from various tissues or organs, and depending on how strict the isolation selection criteria are, some heterogeneity can be introduced by this choice of source. For example, MSCs have been sourced from bone marrow, adipose tissue (AT), umbilical cord blood, umbilical cord tissue, and tonsil.[12, 29] Comparative studies showed AT and umbilical cord blood-sourced MSCs showed higher colony frequency and better proliferation capacity, respectively, compared with BM-MSCs.[30] Phenotypically, ADSCs express CD34, whereas BM-derived MSCs do not.[31] Because of these different characteristics from stem cell types, stem cells isolated from various tissues (bone marrow, adipose tissue, tonsil) were selected in this study for identifying the evaluation technique base on the electrotaxis analysis as a wide use to stem cell homogeneity evaluation.

In Fig. 24, all 3 types of stem cells, hMSC, ADSC and TMSC showed the expression of RUNX2 which represented the osteogenic differentiation marker at day 7, 14. Figure 25 showed that migration speed of all 3 types of differentiated cells was significantly decreased at OsD day 7, 14 however the electric current had no effect on the migration speed. These results

suggested that the electric current effected on only the directional migration of stem cells and 0 differentiated cells, so electrotaxis analysis has the possibility of using to the scell homogeneity evaluation.

For cell quality control by electrotaxis, it is very important that the electric treatment should not affect to differentiation and viability of stem cells. For these reason, post-electrotaxis experiments were performed. We identified that there was no effect of 1000 μA of electric current on the osteogenic differentiation of ADSC, hMSC, TMSC. The viability of stem cells after 1000 μA of electric current was also checked and as a result, stem cell viability was not affected by 1000 μA of electric current (Fig. 26). These data strongly assured that electrotaxis is good candidate for safe method of stem cell quality control.

To distinguish the stem cell and differentiated cells, Youden index of migration speed under electrotaxis was used. Generally Youden index is used to evaluate biomarker levels in the investigation and diagnosis of disease. Disease diagnosis by biomarkers is dependent upon a correlation between biomarker levels and disease state, whereby biomarker levels for a certain diseased population are different–usually higher–than in the corresponding non-diseased

population.[32,33] Figure 24 showed the more osteogenic differentiation progressed, the more migration-speed decreased so stem cell homogeneity is dependent upon a correlation between migration speed and osteogenic differentiation state. In order to utilize migration speed for such classification, a cut-point is established and individuals with migration speed values on one side of the cut-point are labeled as stem cells and those with values on the other side are labeled osteogenic differentiated cells.

Figures 27~29 showed that the mixture ratio 7:3, 5:5, 3:7 of stem cells and OsD cells was matched with the homogeneity evaluation data based on electrotaxis analysis. In OsD 3d, it was hard to distinguish the stem cells and OsD 3d cells by fluorescence markers because only CD-105 was detected and RUNX2 was not (Fig. 27A~C, 28A~C, 29A~C). Similarly, the electrotaxis analysis data showed no different patterns between stem cells and OsD 3d (Fig. 27J, 28J, 29J). However, stem cells showed red dyes (CD-105) and OsD 7, 14d cells showed green dyes (RUNX2) so the distinguishing of stem cells and OsD cells was possible (Fig. 27D~I, 28D~I, 29D~I). The electrotaxis analysis data also showed different pattern between stem cells and OsD 7, 14d cells that the more OsD cells increased, the more low migration speed cells

increased too (Fig. 27K,L, 28K,L, 29K,L). Figure 30 showed that the percentage of stem cells which was calculated using cut-off value was matched with the mixture ratio. These results suggested that OsD took time at least more than 3 days and stem cells moved slower when they started to become OsD cells. This is the key characteristic for stem cell quality control based on the electrotaxis analysis.

According to all results in this study, our stem cell homogeneity technique base on electrotaxis analysis evaluated the stem cell population in culture condition without any specific antibodies so this technique might be used as the stem cell quality control during stem cell culture. Also stem cells which were isolated from various tissues showed common results with this technique, so our evaluation tool could be the wide use to stem cell homogeneity evaluation.

5. Conclusion

Our study demonstrates the possibility about evaluation of stem cell population by the electrotaxis analysis. The mixture ratio of MSCs and osteogenic differentiated cells was almost matched with the distinguishment of MSCs by the electrotaxis analysis. Our study emphasizes the importance of electric current in stem cell migration analysis because the presence of the electric current made more accurate result of discrimination between MSCs and osteogenic differentiated cells. Our result might be used as the new method to evaluate the homogeneity of stem cells.

References

1. Ankrum J, KarpJM. Mesenchymal stem cell therapy: Two steps forward, one step back. Trends Mol Med 2010;16:203-9.

2. Phinney DG, Prockop DJ. Concise review: mesenchymal stem/multipotent stromal cells: the state of transdifferentiation and modes of tissue repair – current views. Stem Cells 2007;25:2896-902.

3. Roh K. Biomanufacturing of therapeutic cells: state of the art, current challenges, and future perspectives. Annu Rev Chem Biomol Eng 2016;7:455-78.

4. Stewart MH, Bosse M, Chadwick K. Clonal isolation of hESCs reveals heterogeneity within the pluripotent stem cell compartment. Nat Methods 2006;3:807-15.

5. Isacson O, Bjorklund LM, Schumacher JM. Toward full restoration of synaptic and terminal function of the dopaminergic system in Parkinson's disease by stem cells. Ann Neurol 2003;53:S135-46.

6. Carson CT, Aigner S, Gage FH. Stem cells: The good, bad and barely in control. Nat Med 2006;12:1237-8.

7. Roy NS, Cleren C, Singh SK. Functional engraftment of human ES cell-derived dopaminergic neurons enriched by coculture with telomerase- immortalized midbrain astrocytes. Nat Med 2006;12:1259-68.

8. Kantor AB, Roederer M. FACS analysis of leukocytes in Handbook of Experimental Immunology. Herzenberg ed. Oxford(OC): Blackwell Science; 1996.

9. Baumgarth N, Roederer M. A practical approach to multicolor flow cytometry for immunophenotyping. J Immunol Methods 2000;243:77-97.

10. Miltenyi S, Muller W, Weichel W. High gradient magnetic cell separation with MACS. Cytometry 1990;11:231-8.

11. Kim, MS. Control of neonatal human dermal fibroblast migration on poly(lactic-co-glycolic acid)-coated surfaces by electrotaxis. J. Tissue Eng. Regen. Med., doi:10.1002/term.1986 (2015).

12. Park YS. Differentiated tonsil-derived mesenchymal stem

cells embedded in matrigel restore parathyroid cell functions in rats with parathyroidectomy. Biomaterials 2015; 65:140-52.

13. Pu J, Zhao M. Golgi polarization in a strong electric field. J Cell Sci 2005;118:1117-28 (2005).

14. Kim, MS. Golgi polarization plays a role in the directional migration of neonatal dermal fibroblasts induced by the direct current electric fields. Biochem Bioph Res Co 2015;460:255-60.

15. Ronen F, David F, Benjamin R. Estimation of the Youden Index and its Associated Cutoff Point. Biometrical J 2005;47:458-72.

16. Greiner M, Pfeiffer D, Smith RD. Principals and practical application of the receiver operating characteristic analysis for diagnostic tests. Prev Vet Med 2000;45:23-41.

17. Pittenger MF. Multilineage potential of adult human mesenchymal stem cells. Science 1999;284:143-7.

18. Dennis JE, Charbord P. Origin and differentiation of human and murine stroma. Stem Cells 2002;20:205-14.

19. Caplan AI. Review: mesenchymal stem cells: cell-based reconstructive therapy in orthopedics. Tissue Eng 2005;11:1198-211 (2005).

20. Rochefort GY. Multipotential mesenchymal stem cells are mobilized into peripheral blood by hypoxia. Stem Cells 206;24:2202-8.

21. Wagegg M, Gaber T, Lohanatha FL, Hahne M, Buttgereit F. Hypoxia Promotes Osteogenesis but Suppresses Adipogenesis of Human Mesenchymal Stromal Cells in a Hypoxia-Inducible Factor-1 Dependent Manner. Plos One 2012;9:e46483.

22. Hung SP, Ho JH, Shih YV, Lo T, Lee OK. Hypoxia Promotes Proliferation and Osteogenic Differentiation Potentials of Human Mesenchymal Stem Cells. J Orthop Res 2012;1:260-6.

23. D'Ippolito G, Diabira S, Howard GA, Roos BA, Schiller PC. Low oxygen tension inhibits osteogenic differentiation and enhances stemness of human MIAMI cells. Bone 2006;39:513-22.

24. Fehrer C, Brunauer R, Laschober G, Unterluggauer H,

Reitinger S. Reduced oxygen tension attenuates differentiation capacity of human mesenchymal stem cells and prolongs their lifespan. Aging Cell 2007;6:745-57.

25. Holzwarth C, Vaegler M, Gieseke F, Pfister SM, Handgretinger R. Low physiologic oxygen tensions reduce proliferation and differentiation of human multipotent mesenchymal stromal cells. BMC Cell Biol 2011;11:11-22.

26. Zhao Z. Directed migration of human bone marrow mesencymal stem cells in a Physiological direct current electric field. Eur Cell Mater 2011;22:344-58.

27. Zhang, J. et al. Electrically Guiding Migration of Human Induced Pluripotent Stem Cells. Stem Cell Rev., doi:10.1007/s12015-011- 9247-5 (2011).

28. Hammerick KE, James AW, Huang Z, Prinz FB, Longaker MT. Pulsed direct current electric fields enhance osteogenesis in adipose-derived stromal cells. Tissue Eng Part A 2010;16:917-31.

29. Secunda R. Isolation, expansion and characterisation of mesenchymal stem cells from human bone marrow, adipose tissue, umbilical cord blood and matrix: a

comparative study. Cytotechnology 2015;67:793-807.

30. Kern S, Eichler H, Stoeve J, Kluter H,Bieback K. Comparative analysis of mesenchymal stem cells from bone marrow, umbilical cord blood, or adipose tissue. Stem Cells 2006;24:1294-301.

31. De Ugarte DA, Morizono K, Elbarbary A, Alfonso Z, Zuk PA. Comparison of multi-lineage cells from human adipose tissue and bone marrow. Cells Tissues Organs 2003;174:101-9.

32. Yin J, Samawi HM, Linder D. Improved Estimation of Optimal Cut-Off Point Associated with Youden Index Using Ranked Set Sampling. Biom J 2008;3:419-30.

33. Yin J, Samawi HM, Linder D. Improved nonparametric estimation of the optimal diagnostic cut-off point associated with the Youden index under different sampling schemes. Biom J 2016;58:915-34.

Abstract (in Korean)

물리적 자극을 이용한 세포 이동 조절의 조직공학적 이용

<지도교수 박종철>

연세대학교 대학원 의과학과

김 민 성

조직공학 분야는 수많은 장기와 조직의 수요를 충족시키기 위해 발전되어 왔고 보편적으로 인체의 살아있는 장기의 대체품을 제작하고는 것에 초점이 맞춰져 있다. 많은 연구들이 생체재료를 이용한 지지체를 제작하기 위해 행해지고 있다. 이러한 지지체는 세포외기질과 세포들이 3차원 구조체를 형성하고 원하는 조직을 구성할 수 있도록 성장하는데 도움을 준다. 조직재생을 위한 이상적인 지지체의 조건은 적절한 기계적 강도를 지니고, 조직 주변부분과의 생체적합성이 높아야 하며, 다공성의 성질을 가지면서도 조직이 재생됨에 따라 점차적으로 생체 내에서 분해가 되어야 한다 이러한 요건을 충족하기 위해서는 지지체에 세포들이

넓고 고르게 분포되어 있어야 하는데 이를 위해서 세포 이동의 조절이 필요하다. 또한 조직공학에서 줄기세포의 적용이 많이 연구되고 있는 상황인데 현재 줄기세포 분화 방법이나 배양방법에서는 세포의 동질성을 보장하기 어렵기 때문에 세포의 동질성을 평가하는 방법이 필요하다.

유체의 흐름에 의한 전단응력의 경우 유체의 흐름 방향으로 hMSC의 이동을 2-D 상태에서 유도하였고, 그 때에 골지체를 BFA로 억제시킴으로써 유체 흐름의 전단응력에 의한 세포이동 유도와 골지체의 상관관계를 확인하였다. 3-D PLGA 지지체에 유속에 의한 전단응력을 가해주었을 때 hMSC의 지지체 안으로의 이동이 증가하는 것을 확인하였고 이 때에 물리적인 힘이 아닌 전단응력에 의해 세포가 능동적으로 움직일 수 있는 mechanotransduction과 관련된 움직임을 보인다는 것을 확인하였다. 전기자극에 의한 세포이동 유도의 경우 hMSC는 전기자극의 +극 방향으로 움직이는 것을 확인하였고 3-D 지지체에 전기자극을 흘려주었을 때 역시 지지체 안쪽으로 전류의 흐름에 따라 세포의 이동이 증가함을 확인하였다.

세포의 동질성 확인과 관련된 연구로써 지방유래 중간엽 줄기세포, 골수유래 중간엽 줄기세포, 갑상선 유래 줄기세포가 사용되었는데 이 세 종류의 줄기세포 모두 전기자극에 의해 + 극으로 이동이 유도되고, 세 종류의 세포 모두 골분화 진행과정이 7일 이상 지남에 따라 세포이동 속도가 현격히 감소하는 것을 관찰하였다. 이를 토대로 세포이동 속도를 기반으로 하여 줄기세포와 골분화 진행 과정중의 세포의 분포 정도를 확인할 수 있었다.

이번 연구를 통하여 유체의 흐름에 의해 생기는 전단 응력이나 전기 자극과 같은 세포 외부에서 가해주는 자극으로 세포의 이동을 조절 가능한 조건을 확립하고 궁극적으로 외부 자극을 이용해서 지지체 속으로 세포가 충분히 침투되지 못하는 문제 해결의 가능성을 확립하였고, 세포이동 분석을 이용한 세포의 동질성을 평가할 수 있는 새로운 방법을 제시하였다.

핵심되는 말: 세포이동, 3-D 지지체, 조직공학, 줄기세포, 전기주성, 유체의 전단응력, 세포동질성